

Notes on

GEOMETRIC PROCESSING OF REMOTE SENSING IMAGES

F. Leberl

Guest lecturer, ITC



INTERNATIONAL INSTITUTE FOR AEROSPACE SURVEY AND EARTH SCIENCES

Notes on

GEOMETRIC PROCESSING OF REMOTE SENSING IMAGES

F. Leberl

Guest lecturer, ITC

M.Sc. course photogrammetry (P2)

ITC

Enschede, February 1984

ITC-P2-Course

Remote Sensing

10 hrs

Purpose:

- To enhance the understanding of geometric aspects of non-conventional imaging,
- to present an opinion on the applications of satellite data to conventional mapping and
- to present ideas on remote sensing applications in the mapping environment.

Prerequisite:

Knowledge of the basics of remote sensing (ITC standard course on remote sensing or equivalent).

Contents:

Discussion of current and planned remote sensing satellite systems (Landsat TM, SPOT, Shuttle-missions, ERS-1) and of aircraft systems (MSS, thermal, radar).

Projection equations for scanning and radar, with linearized forms. Scan and radar imaging geometry from satellite platforms. Resection and intersection with remote sensing images.

Geometric and radiometric rectification of radar and scan images, using digital elevation models. Stereoscopic viewing and height measurements with scanning (linear array) and radar sensors. Scan and radar image blocks (optional).

Relating aircraft and satellite remote sensing data to conventional mapping requirements.

1. REVIEW OF BASICS OF REMOTE SENSING

Remote sensing for a photogrammetrist is the work with scanning and radar images. A complete definition can be found on pp 1 - 3 of the P1 lecture notes. The following is a review of the P1-material on generating scan- and radar images.

1.1 Scanning

a. Thermal mapping

Scanning was invented to create thermal images. The principle was discussed in the P1-lecture notes. Originally one was only using one bulky detector that needed cooling. The scan operation is (was) in both directions, along and across the flight direction. The mirror rotation served for cross-track scans, the aircraft or spacecraft motion served for along-track scanning.

b. Multispectral imaging

Scanning was soon extended from the thermal domain to the photographic portion of the electro-magnetic spectrum (UV, visible, photographic infra-red). The reason was that agricultural scientists expected to be able to automatically classify the image contents based on spectral information alone. The scanner (see Fig. 2.8 in the P1-lecture notes) promised to provide for a much narrower and accurate spectral resolution than a camera with given filters and color film. Also it promised to produce data more easily submitted to automated analysis based on 'multi-spectral sensing' (MSS).

These arguments were unrelated to satellite operation. Numerous aircraft experiments were flown, instruments developed and research reports published. The Laboratory for the Application of Remote Sensing (LARS) clearly was the leading institution.

Today aircraft multi-spectral sensing is not being discussed anymore, except to support satellite remote sensing research, or to use only the thermal channel for heat mapping.

c. Spectral Information and Logistics

The spectral information has not proven to be of much central value; an aircraft MSS system suffers from superior colour photography competition due to its better geometric properties.

In satellite systems (Landsat-MSS, Nimbus, Tiros, Landsat Thematic Mapping, SPOT) scanning is superior to photography due to the transmission of images to the ground. There is therefore a great logistics advantage for satellite scanning over space photography.

The spectral information value is limited in the view of SPOT-designers: only 3 spectral bands are available, just as in colour photography.

The U.S. agency NASA still is in favour of high spectral resolution: Landsat 5 (launch 1 March 1984) will have the thematic mapper with 6 spectral bands. A series of space shuttle experiments is under way to test "very high spectral resolution" capabilities with 100 or so spectral bands.

d. Optical-mechanical versus linear array scanning

The scanning mirror systems such as those in Landsat represent "optical-mechanical scanning". This leads to peculiar geometric problems, bulky instruments and difficulties in space operations.

"Push-broom scanning" is based on linear arrays of minute detectors. The system operates much like the military's strip camera where an open, fixed exposure slit is equipped with say, an array of 5000 detectors (charge-coupled devices, CCDS, etc.).

Advantages are:

- nothing moves, therefore the satellite operation is easier
- the system is more compact
- the exposure time per image element is much longer than with optical-mechanical scanning
- the geometry is simpler than that of optical-mechanical scanning.

The most important factor is exposure time. With a rotating mirror at 6000 r.p.m. one has 100 image lines per second. (In a satellite this is 70 m per image line, since it moves at 7 km/sec). If in one line 3000 image points need to be generated then the detector could look at the object for a mere 1/300.000 seconds! The push-broom concept allows for a full 1/100 second for each point on an image line, leading to much better contrast and signals.

e. Other types of scanning

Numerous other scanning concepts have been proposed. Apart from the common scan operation in a vertical plane one may have scans in inclined planes, cones with horizontal or with vertical axes.

The latter system of conical scanning was proposed for the advantages of equal incidence angles for each object: one does not look vertically onto the nadir and at some angle to the side, but one always is looking towards the side.

Scanning in an inclined plane is proposed for future stereo systems where one could look forward and backward and thereby can obtain a convergent stereo concept. This is part of the proposals for STEREOSAT and for MAPSAT.

f. Spatial resolution, scale

Reference is made to Figs. 2.9 and 2.10 of the P1 lecture notes.

1.2. Radar imaging

a. Active systems

A full description of "active mapping" and of so-called "real aperture radar" imaging was presented in chapter 2.3 of the P1 lecture notes. It included an enumeration of advantages and disadvantages or resolution and image scale.

b. Synthetic aperture radar

A description of synthetic aperture radar is beyond the scope of the course; it should be noted only that ground resolution is independent of the distance to the object. Satellite radar is with synthetic aperture radar (SAR).

c. Imaging systems

Land image mapping is operational since 1967. Satellite radar so far was with

- SEASAT (3 months in 1978)
- Space Shuttle Imaging Radar (SIR-A) 1981
- expected missions are with the shuttle (SIR-B) and on a European satellite (ERTS-1).

d. Properties of radar images

Examples of radar images to be discussed in the course are:

- image of the gateway arch in St. Louis (USA)
- image of tailing ponds and of open-pit mining in Arizona (USA)
- comparison of Landsat MSS band 7 of a tropical jungle with an aircraft SAR
- Seasat-SAR image of Los Angeles
- aircraft real aperture images of the pacific coast of Colombia
- effect of heavy rains on an image with 3 cm wavelengths
- the concept of 'fore-shortening'
- the image of a tower and with mirror reflections
- radar penetration in snow and ice
- diffuse and granular reflection
- bi leadral tri leadral reflectors
- image of houses
- image of an island
- stereo image pair
- radar derived contour lines
- convergent flight lines with satellites
- SIR-A images of Cephalonia stereopair.

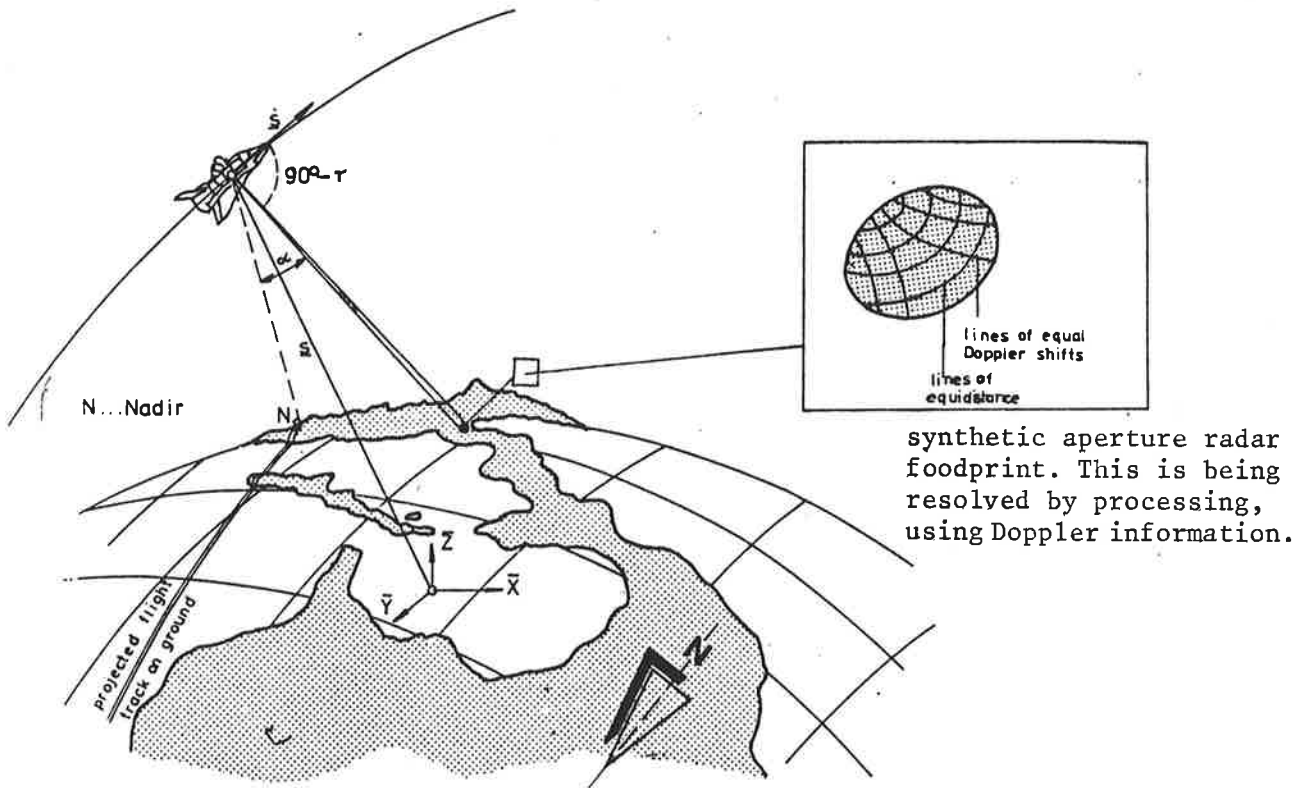


Figure 1.1 : Radar imaging from orbit, where \underline{s} is the position vector of the sensor.

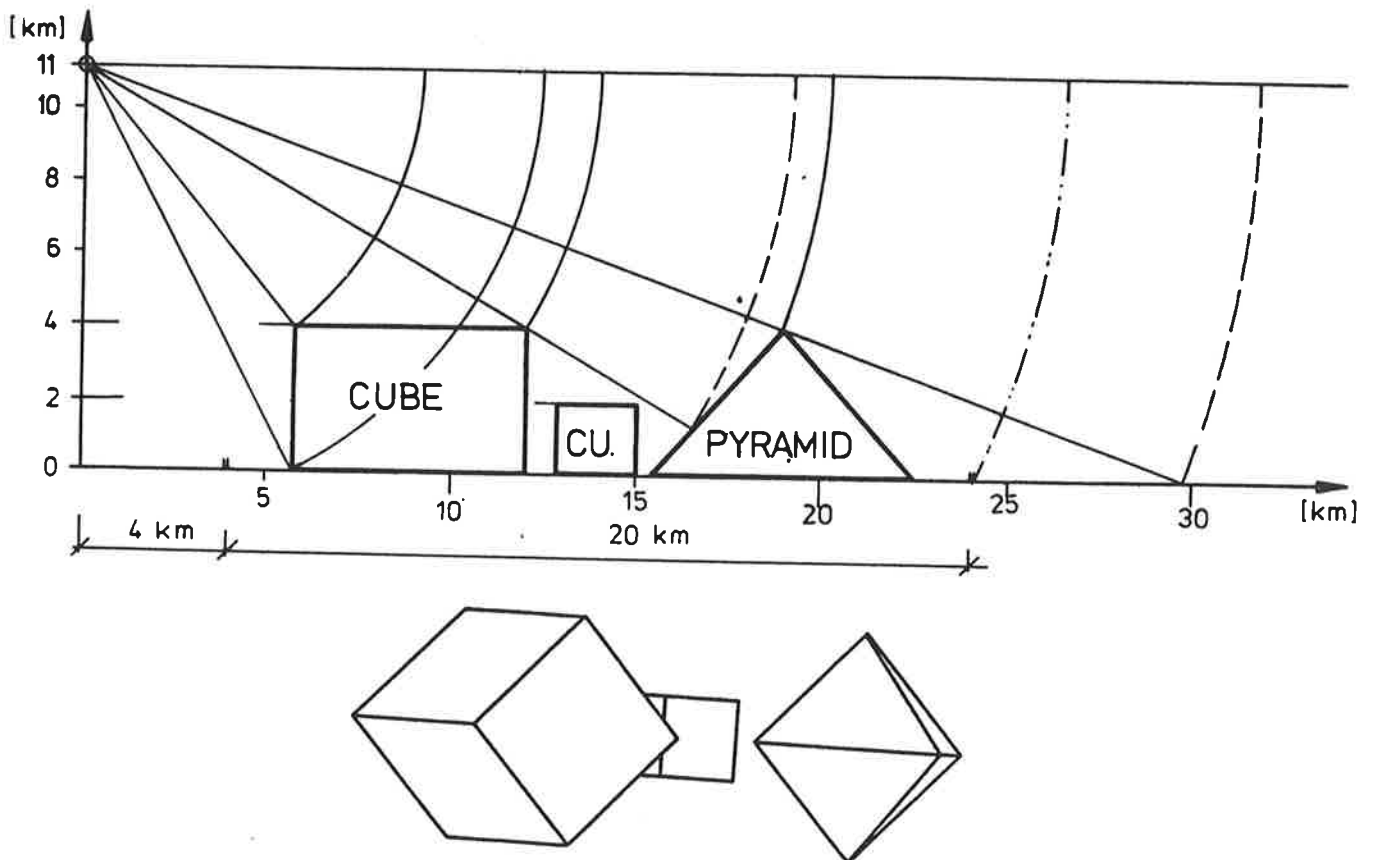


Figure 1.2: Imaging arrangement (above) and radar image shapes (below)

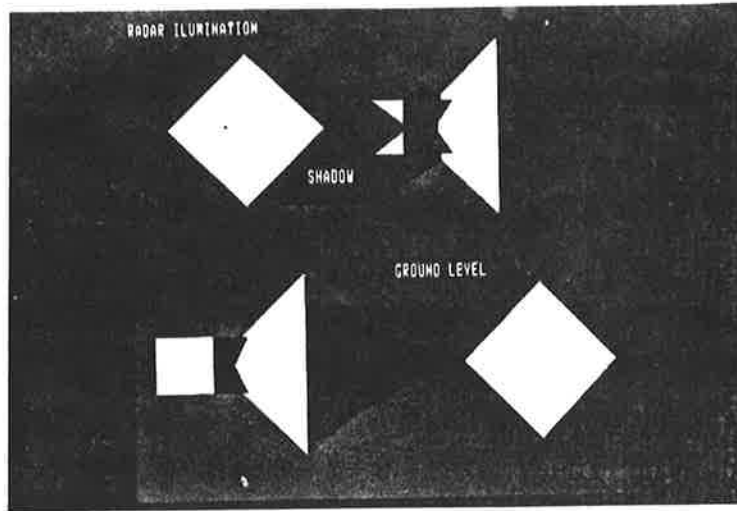


Figure 1.4.a: Radar illuminated height model (shadow and illuminated areas can be clearly separated).

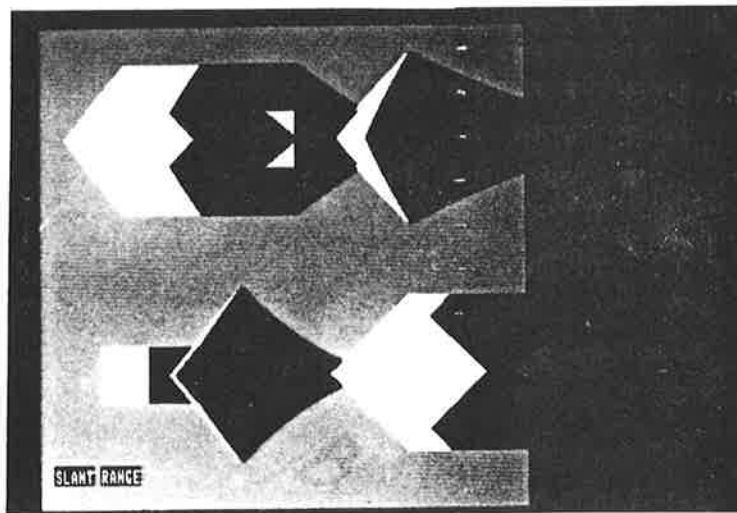


Figure 1.4.b: Radar slant range presentation.

e. Outlook on radar imaging

It is fairly obvious that the geometric resolution of radar imaging will not advance significantly in the future: today 3 m resolution cells could be available and are being generated by a few systems. Still the majority of applications does rely on 10 m at 20 m resolution data.

Satellite radar will be available towards the end of the decade, simply due to the need of overcoming weather constraints. The extent to which this will penetrate into specific applications is still widely unclear.

1.3. Other imaging systems

a. SONAR images

Compare Fig. 2.18 of P1 lecture notes.

b. Passive microwave sensing

Temperature measurements for meteorological purposes are based on satellite microwave sensing. Emitted microwave energy is saved by a scanning antenna. The scan can be circular. Received intensity of radiation is proportional to the emitting object.

2. GEOMETRIC PROCESSING BASICS OF REMOTE SENSING IMAGES

Specific methods have been developed in the past for geometric work on remote sensing images. These techniques depend on:

- geometric resolution
- type of imagery
- application
- the availability of single images, stereopairs or image blocks.

The most trivial problem is with single images at poor resolution, e.g., a LANDSAT-MSS image, that needs to be related to a map.

A more complex problem is the set-up, and plotting from, a stereo radar image pair on an analytical plotter.

The range of problems can be split into separate elements. These are:

- "non-parametric" techniques of image rectification
- parametric models of image geometry (projection equation)
- parametric explanation of systematic image deformations
- (- given a set of control points and an image, find the exterior orientation of the sensor ("resection in space"))
- given an image with the exterior orientation, find the ground coordinates of identified image points
- given the image with exterior orientation, and given an object point, find its location in the image
- for a given image, exterior orientation and digital height model of the terrain, generate an ortho-image
- with an overlapping pair of images and a stereoscope with parallax bar, generate measurements of height and slope
- with an overlapping pair of images and an analytical plotter, create an oriented stereo-model and plot from it in real time
- with a block of overlapping images and with both control- and tie-points, create a dense grid of minor control points for subsequent ortho-image generation and photo-mosaicing.

If we also consider the above tasks to be studied for aircraft and spacecraft remote sensing with optical-mechanical linear array scanning and with radar, we quickly see an enormous range of challenging work to be done.

We will discuss some of the tasks required to approach the listed tasks. There is finally still the broad category of digital image processing. Geometric aspects follow the resolution of certain photogrammetric problems, such as:

- generating a rectified image by resampling
- registration of two images by means of image correlation
- mosaicing of images using image correlation and grey value matching.

2.1. Non-parametric techniques of image rectification

A synonymous expression is "interpolative". One defines ΔX_0 ΔY_0 image deformations in control points (GP_s). This is achieved by some form of simple transformation. In any new image point x_p, y_p one then has to interpolate corrections Δx_p Δy_p on the basis of the known Δx_c Δy_c values.

The following will review some of the most widely used techniques. A complete discussion of methods relevant in this context is in the framework of the "Transformation and Interpolation" course in P1/P5.

a. Input for non-parametric methods

We do not need flight data, nor do we have to understand the type of sensor or sensor geometry. We simply use a set of ground control points with their planimetric coordinates X_G, Y_G . The height coordinate is not considered. In the image one has to identify the same points and obtain their coordinates x, y . We therefore have as input:

Point number PN	Ground or Map		Image	
	X	Y	X	Y
1	3428.3	2197.4	34.74	-16.23
2	9713.9	-2940.3	-21.10	428.13
3
.
.
.

b. Linear conformal transformation

See Appendix A for a summary of the method. There is hardly a set of images that can be successfully processed with just this transformation. Generally one has at least to expect a scale differential along and across track (along = in flight at x ; across is at 90° angle = y).

c. Affine transformation and higher order polynomials

See Appendix A for a discussion. Any type of higher order transformation needs to be carefully planned (see end of appendix A). The use of such transformation is typical of simple rectification systems used with LANDSAT-MSS. Application is acceptable only with low accuracy requirements and high control point density.

d. Collineation

In the event of Landsat RBV of flat areas we can model the projection by collineation. This is also a valid method of non-parametric processing (see appendix A).

e. Interpolation after transformations

Appendix B describes several methods of interpolating Δx_n , Δy_n values in new points n from the known Δx_c , Δy_c residuals at control points from the transformation.

2.2. Parametric models of image geometry

a. General

It is very rare that one finds in the remote sensing field work using correct mathematical descriptions of the sensing geometry when in fact this is not really of any great complexity.

We know the camera case as reviewed in Appendix C. However, in a more general sense, we can define a similar projection equation also for a dynamically scanning sensor as follows:

$$\underline{p} = \underline{0} + \underline{p}^* \quad (2.1)$$

$$\underline{p}^* = \underline{A} \underline{p}_a$$

\underline{A} ... rotation matrix $\underline{A}(t)$

\underline{p}_a .. sensor space vector

$\underline{0}$... position vector of sensor, $\underline{g}(t)$

b. Differentiate the general equation

$$\underline{p}_a = \underline{A}^{-1} (\underline{p} - \underline{s}) = \underline{B} (\underline{P} - \underline{s}) \quad (2.2)$$

$$\underline{p}_a \text{ corrected} = (\underline{B}) d\underline{B} (\underline{p} - \underline{s} - d\underline{s}) = (\underline{B}) (\underline{E} + d\underline{M})(\underline{p} - \underline{s} - d\underline{s})$$

$$\underline{p}_a \text{ corrected} = \underline{p}_a + d\underline{p}_a = (\underline{B})(\underline{p} - \underline{s}) + (\underline{B}) d\underline{B} (\underline{p} - \underline{s}) - (\underline{B}) d\underline{s} + \dots$$

$$d\underline{p}_a ; d\underline{M} \underline{p}_a - \underline{B} d\underline{s}$$

where

$$d\underline{M} = \begin{bmatrix} 0 & -d\kappa & d\phi \\ d\kappa & 0 & -d\omega \\ -d\phi & d\omega & 0 \end{bmatrix}$$

c. We specialise for scanning

From figure 3.1. we read:

$$\underline{p}_a = \lambda (0, c \cdot \tan \Omega, -c) \quad \begin{array}{l} c = \text{principal distance} \\ \Omega = \text{look angle} \end{array} \quad (2.3)$$

For "exotic" scanning we need to consider the following cases:

A is split into A₁ and A₂:

$$\underline{p} = \underline{s} + \underline{A}_1 \cdot \underline{A}_2 \cdot \underline{p}_a$$

where A₁ is the orientation matrix: A₂ is auxiliary.

Vertical plane:

$$\underline{A}_2 = \underline{E}; \underline{p}_a = \lambda (0, c \cdot \tan \Omega, -c)$$

Conical scan

$$\underline{A}_2 = \underline{E}; \underline{p}_a = \lambda (c \tan \phi_0 / \cos \Omega, \tan \Omega, -c)$$

Circular scan

$$\underline{A}_2: \phi = 90^\circ, \omega = \kappa = 0; \underline{p}_a \text{ as in conical scan.}$$

Inclined plane

$$\underline{A}_2: \text{arbitrary. } \underline{p}_a \text{ as in vertical plane.}$$

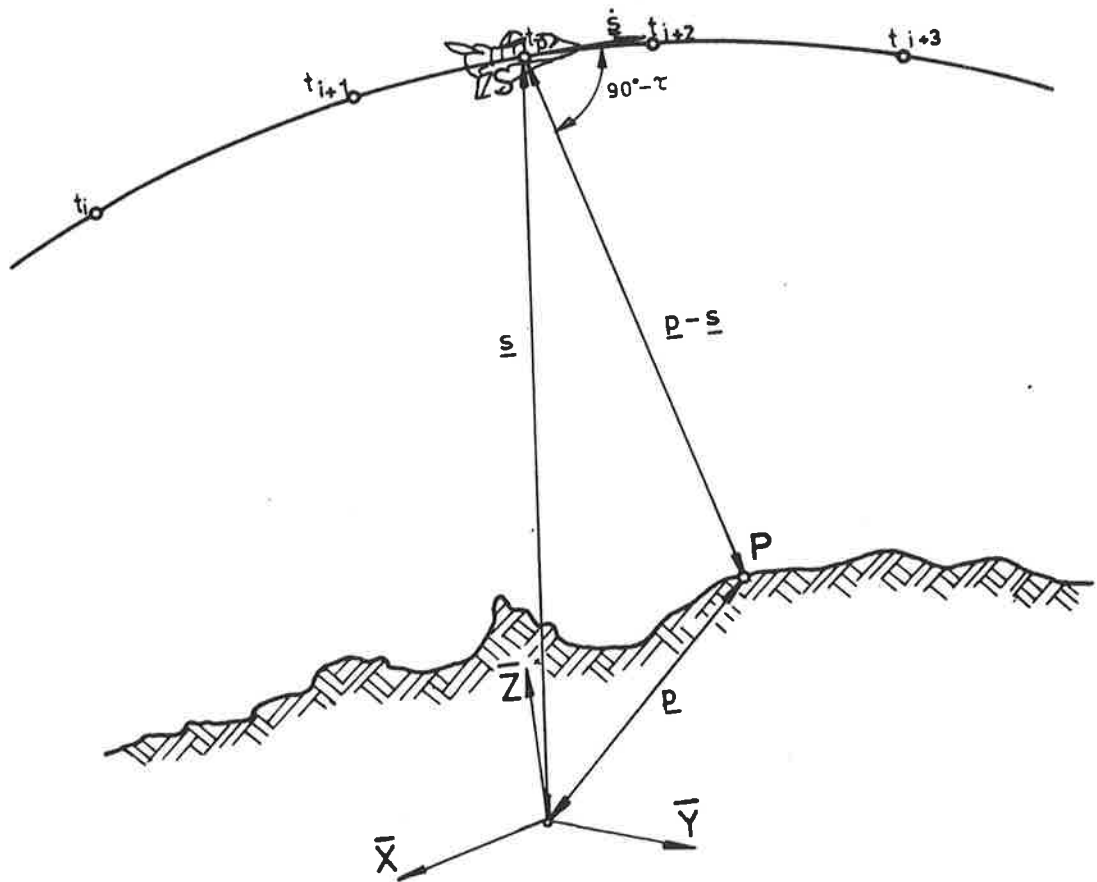


Figure 2.0: Relating image to object.

d. Relating Pa to an image x,y system

$$x,y \leftrightarrow \underline{Pa} \quad (x,y) \leftrightarrow (u,v,w)?$$

(2.4)

$$x = v_{\text{film}} = \text{time}$$

$$y = v, \text{ but curved film}$$

$$y = \Omega \cdot c$$

$$\Omega = \arctan v/w$$

$$y = c \cdot \arctan (v/w)$$

e. We specialize for radar

With slant image r , elevation angle Ω and squint angle Φ_0 Figure 3.2. shows:

$$\underline{Pa} = r \{ \sin \Phi_0, (\cos^2 \Phi_0 - \cos^2 \Omega), -\cos \Omega \} \quad (3.5)$$

$$1. u^2 + v^2 + w^2 = (X - X_0)^2 + (Y - Y_0)^2 + (Z - Z_0)^2 = r^2 \quad (3.6)$$

$$2. \underline{i} \cdot (\underline{p} - \underline{s}) = \sin \Phi_0 \cdot |\underline{p} - \underline{s}| = \sin \Phi_0 \cdot r \quad (3.7)$$

Equ. (3.7) is a range sphere of radius r , equ. 3.6 is a cone with vertex angle Φ_0 (compare figs. 3.3, 3.4).

f. Relating r and time t to image x,y

$$z = v_{\text{film}} = t$$

$$y = r/\lambda \quad \text{slant image presentation}$$

$$y = (r^2 - Z_0^2)^{\frac{1}{2}} \quad \text{ground range presentation}$$

g. Synthetic aperture radar

No angles ϕ, κ (ω is irrelevant anyway)

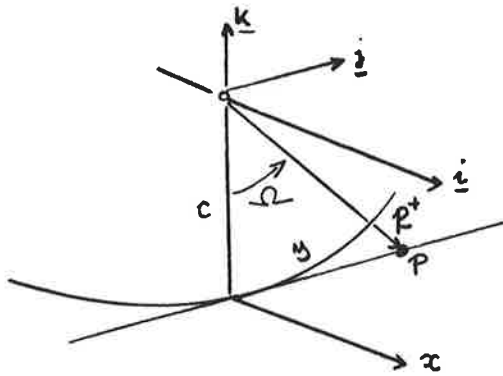
Instead: Velocity vector

$$\underline{i} = \underline{s} / |\underline{s}|$$

\underline{j} = normal onto \underline{i} and the local vertical

$$= \underline{i} \times \underline{s} / |\underline{s} \times \underline{i}|$$

$$k = \underline{i} \times \underline{j}$$



$$\underline{p}^+ = 0.\underline{i} + c \tan \Omega . \underline{j} - c\underline{k}$$

Figure 2.1: Scan geometry

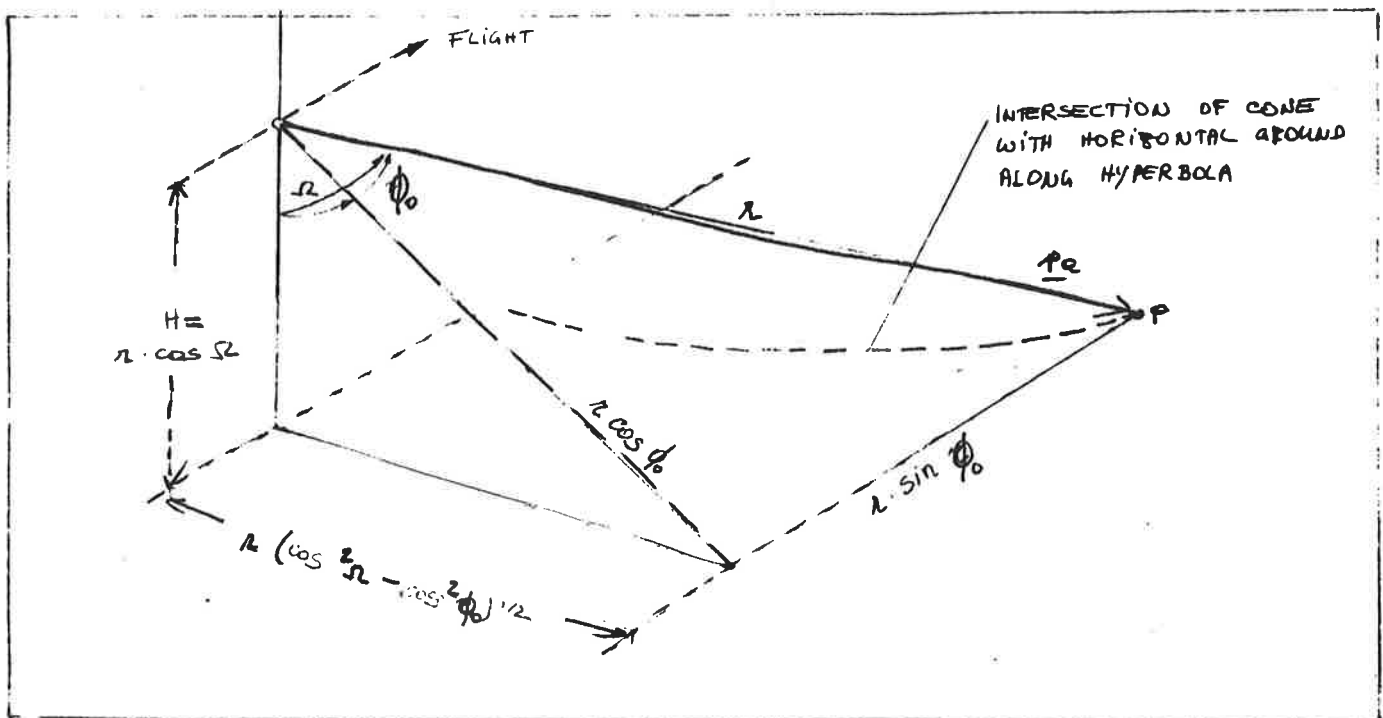


Figure 2.2 : Definition of vector \underline{p}_a for radar

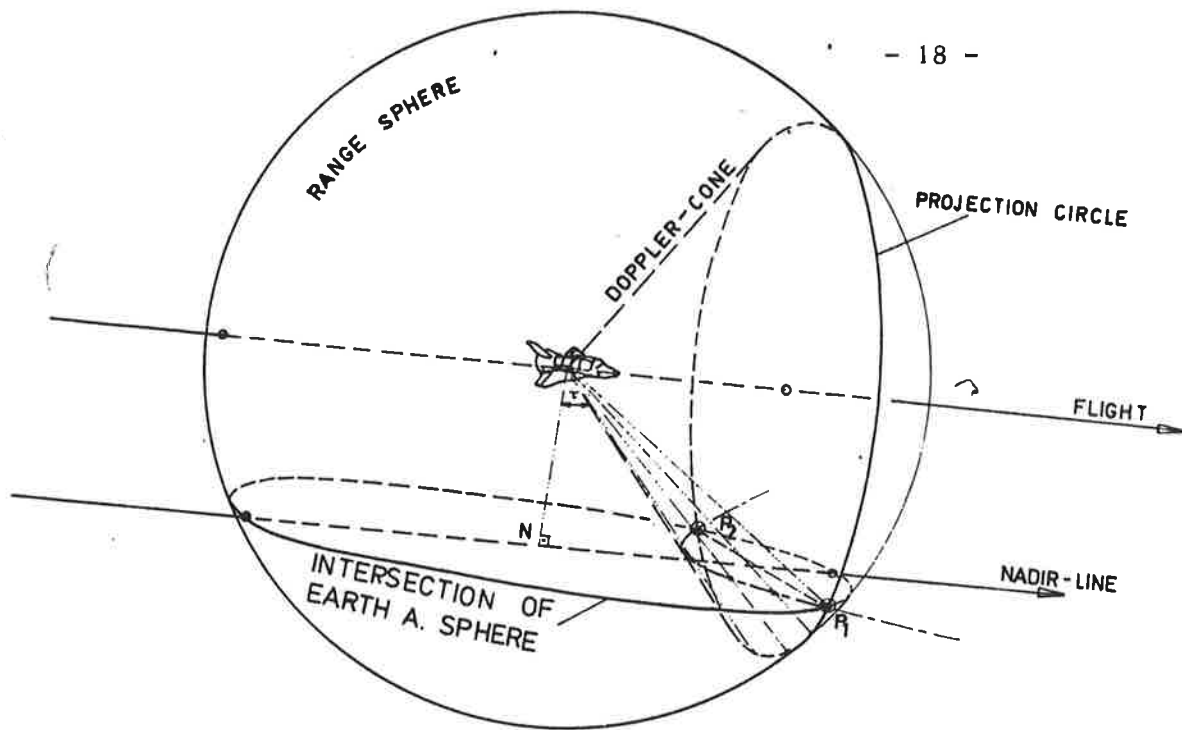


Figure 2.3 : Doppler cone and range sphere.
Perspective view.

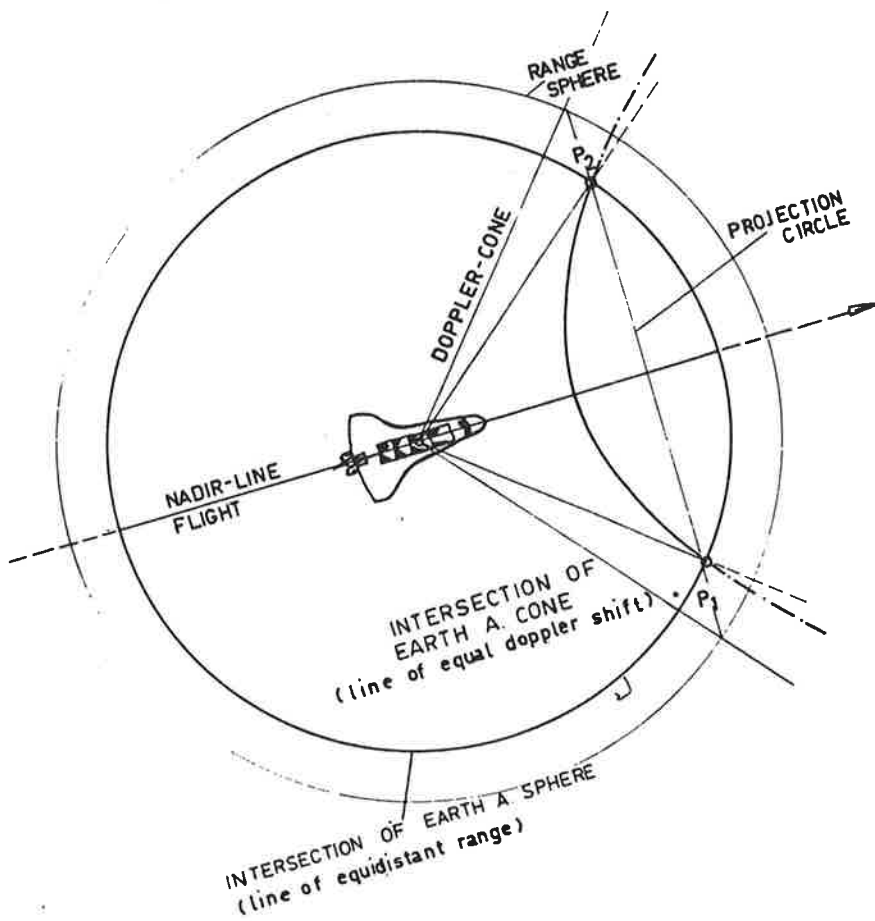


Figure 2.4 : Doppler cone and range sphere.
Vertical view.

2.3. Parametric explanations of systematic image deformation. Differential forms of projection equations

a. Scanning

Common equ. (2.4) on page 12):

$$dy = c \cdot \cos^2 \Omega \{dv/w - dw \cdot \tan \Omega / w\}$$

$$dx = -du$$

$$d\underline{p} = \begin{bmatrix} du \\ dv \\ dw \end{bmatrix} = - \underline{B} ds + d\underline{M} \cdot \underline{p} = - \begin{bmatrix} dX_0 \\ dY_0 \\ dZ_0 \end{bmatrix} + \begin{bmatrix} -vd\kappa + w d\phi \\ ud\kappa - w d\omega \\ -ud\phi + v d\omega \end{bmatrix}$$

With $\underline{B} = \underline{E}$ (unit matrix):

$$\begin{aligned} dx &= -dX_0 + Z_0 d\phi + Z_0 \tan \Omega d\kappa \\ dy &= - \frac{\sin 2\Omega}{2} dZ_0 + Z_0 d\omega - \cos^2 \Omega dY_0 \end{aligned}$$

(2.8)

where $\underline{s} = X_0 \underline{e}_1 + Y_0 \underline{e}_2 + Z_0 \underline{e}_3$

$$d\underline{s} = \begin{bmatrix} dX_0 \\ dY_0 \\ dZ_0 \end{bmatrix}$$

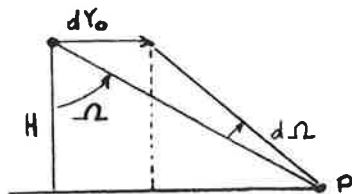
$$w = +Z_0 = -c \cdot \lambda$$

$$v = -Z_0 \tan \Omega$$

$$u = 0$$

$$\lambda = 1$$

A simple derivation of these effects is e.g. With Figure 2.5.



$$y = c \cdot \Omega$$

Figure 2.5: Effect of dY_0 on y .

For $\Omega = Y/H$

$$\frac{dY_0}{H} - \frac{dH \cdot Y}{H^2} = \frac{\cos^2 \Omega + \sin^2 \Omega}{\cos^2 \Omega} d\Omega \quad (2.9)$$

$$d\Omega = \cos^2 \Omega \left\{ \frac{dY_0}{H} - \frac{Y}{H^2} dZ_0 \right\}$$

q.e.d.

b. Radar

$$dx = du$$

$$dy = dr/\lambda = \left\{ \frac{v}{r} dv + \frac{w}{r} dw \right\} / \lambda \quad \text{slant ranges}$$

$$dy = \left\{ \frac{r}{y \cdot \lambda} dr - \frac{Z_0}{y} dZ_0 \right\} / \lambda \quad \text{ground ranges}$$

$$dx = -\Delta X_0 + Z_0 \tan \Omega \cdot d\kappa - Z_0 d\phi \quad (2.10)$$

$$dy = -\cos \Omega dY_0 + \sin \Omega dZ_0 \quad \text{slant ranges}$$

$$dy = -dY_0 + \cos \Omega dZ_0 \quad \text{ground ranges}$$

3. GEOMETRIC PROCESSING TASKS

3.1 RECONSTRUCTION OF THE EXTERIOR ORIENTATION OF A SENSOR (Resection in Space)

(a) Camera

Given are a camera metric photograph with a set of control points and known inner orientation. We need to find the rotation matrix R and the sensor position s. This problem is denoted by "resection in space". It applies to LANDSAT-RBV and all other perspective images.

There exist standard solutions to this problem in photogrammetry. They can proceed essentially as follows:

- (a) an approximate value is assumed or known for \underline{R} and \underline{s} ;
- (b) using the approximate values, a (fictitious) image location $(\bar{x} - x_0), (\bar{y} - y_0)$ is computed for each control point, using equ. A.3;
- (c) for each control point a residual discrepancy is found between the computed values $(\bar{x} - x_0), (\bar{y} - y_0)$ and the actually observed ones $(x - x_0, y - y_0)$. These differences dx, dy , are used as given observations in equ. 6.4 to solve for unknown additions to the approximate values $(\phi), (\omega), (X_0), (Y_0), (Z_0)$;
for x we get: $\bar{x} - x = \frac{c}{H} dX_0 - \frac{x}{H} dZ_0 + c \left(1 + \frac{x^2}{c^2}\right) d\phi - \frac{xy}{c} d\omega - y d\kappa$
This leads to $dX_0, \dots, d\kappa$ and:

$$\begin{aligned} \phi &= (\phi) + d\phi \\ \omega &= (\omega) + d\omega \end{aligned} \tag{3.1}$$

N control points provide us with $2.N$ equations of type A.4. An overdetermined system must be solved with the method of least squares.

(b) Scanners and Radars

The basic method is the same as that for cameras. The "resection" of image points x, y , from known ground control is more difficult. An algorithm will be shown later. The computed image positions \bar{x}, \bar{y} , and measured x, y of a given ground control point define discrepancies dx, dy , which enter again in a linearized equation of the form (2.8) or (2.10).

However, $d\phi, d\omega, d\kappa, dX_0, dY_0, dZ_0$ are 6 unknown additions to approximations that exist at every moment of time t . We have thus a 6 fold infinity of unknown values!

The solution to this dilemma is the definition of functions of time for the unknown values:

$$\begin{aligned} d\phi &= a_0 + a_1 t + a_2 t^2 + \dots \tag{3.2} \\ d\omega &= b_0 + b_1 t + b_2 t^2 + \dots \end{aligned}$$

This leads to $(n+1)$ 6 unknowns, where n is the order of the polynomial used in equ. (3.2) for each unknown sensor attitude or position value.

This solution has been proposed and studied by many authors. It exists in various alternatives. Even unknown parameters of the inner orientation have been computed in this way (c, τ etc).

3.2 CONTROL POINTS

Usually ground control points are used to rectify an image. The points can be manually identified in a map and the image; some workers like to do this by visually superimposing map and image; e.g. with a Zoom-Transferscope.

Handpicked control in an image is certainly the best possible measure of geometric deformation. However, in an image-image correspondence problem this approach is time-consuming.

There exist image-image correspondence methods that are called "image correlation". These automatically compare patches of image gray values in the two images to find maximum similarity. These techniques work well in well textured data. In non-textured images (LANDSAT), such as on water-bodies, forest-photography, desert images, this correlation or similarity detection can fail. Then the human has to support the automated procedure.

One may note that automated methods of image-image correlation can identify incorrectly two points to be corresponding to one-another. Typical errors are due to shadows etc.

Image-image correlation/similarity detection can be for geometric matching or for the purpose of height parallax detection. This in turn can lead to the computation of digital terrain heights, or a DTM (digital terrain model).

3.3 INTERSECTION OF A VECTOR WITH A SPHERE/ELLIPSOID

We assume the satellite orbit to be known:

$$\underline{s}(t) = \text{known}$$

Also the attitude of the satellite is known. We define the sensor coordinate axes as \underline{u} , \underline{v} , \underline{w} :

$$\begin{aligned}\underline{u} &= \underline{\dot{s}} / |\underline{\dot{s}}| & \underline{\dot{s}} & \dots \text{velocity vector} \\ \underline{v} &= \underline{u} \times \underline{s} / |\underline{s}| \\ \underline{w} &= \underline{u} \times \underline{v}\end{aligned}\tag{3.3}$$

With respect to these axes one has measured attitude angles roll, pitch and yaw, leading to a rotation matrix \underline{M} .

\underline{M} = Rotation matrix to correct for pitch, yaw, roll.

The rotation matrix \underline{D} then relates the sensor coordinate system \underline{u} , \underline{v} , \underline{w} into the object system \underline{x} , \underline{y} , \underline{z} ; a combined matrix $\underline{D} \cdot \underline{M} = \underline{F}$ is then the one relating the

sensor into the object system after roll, pitch and yaw are introduced.

We now need to define the line of sight, or position vector \underline{p}^+ of an imaged point in the sensor system. We then get this vector in the object system \underline{p} :

$$\underline{p} = \underline{F} \cdot \underline{p}^+$$

This needs to be intersected with the ellipsoidal surface:

$$\frac{x^2}{a^2} + \frac{y^2}{a^2} + \frac{z^2}{c^2} = 1$$

This can also be represented by:

$$\begin{pmatrix} a \cdot \cos u_1 \cdot \cos u_2 \\ a \cdot \sin u_1 \cdot \cos u_2 \\ c \cdot \sin u_2 \end{pmatrix} = E(u_1, u_2)$$

Where u_1, u_2 are latitude and longitude on the surface.

The position of the intersection point is:

$$L(u) = \underline{s} + u \cdot \underline{p}$$

This is equated with the surface:

$$s_x + u \cdot p_x = a \cos u_1 \cos u_2$$

$$s_y + u \cdot p_y = a \sin u_1 \cos u_2$$

$$s_z + u \cdot p_z = c \sin u_2$$

This is a system of 3 equations with 3 unknowns u, u_1, u_2 . We solve by multiplying the 3rd equation by a/c and squaring all sides of each equation, then adding up everything:

$$\left\{ c^2 (p_x^2 + p_y^2) + a^2 p_z^2 \right\} u^2 + 2 \left\{ c^2 (p_x s_x + p_y s_y) + a^2 s_z p_z \right\} u + c^2 (s_x^2 + s_y^2) + a^2 (s_z^2 - c^2) = 0$$

This is

$$A \cdot u^2 + B \cdot u + C = 0$$

and

$$u = \frac{-3 - \sqrt{B^2 - 4AC}}{A}$$

Note that the negative of the root is selected, because we accept the nearer intersection as the solution. Finally

$$\underline{X} = \underline{s} + u \underline{p}$$

3.4 INTERSECTION OF A RADAR PROJECTION LINE WITH AN ELLIPSOID

We have:

$$|\underline{p} - \underline{s}| = r \quad \text{Range sphere}$$

$$\frac{x^2 + y^2}{a^2} + \frac{z^2}{c^2} = 1 \quad \text{Earth}$$

$$\tan \tau = u / \sqrt{v^2 + w^2} \quad \text{Doppler cone}$$

or

$$\underline{u} = 0$$

(a) With a sphere

The solution is shown in Figure 3.1.

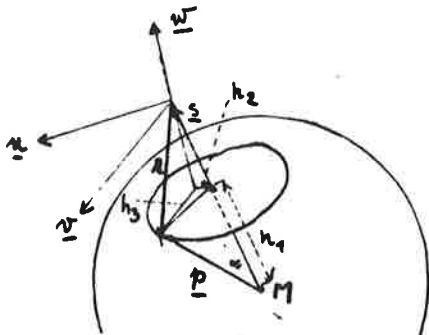


Figure 3.1: Intersection of radar projection line with sphere

$$h_1 = \underline{s} h_1 / s$$

where

$$h_1 = (R^2 + s^2 - r^2) / 2s$$

$$\begin{aligned} & \text{(cosine rule: } r^2 = R^2 + s^2 - 2Rs \cos \alpha \\ & \text{but } R \cos \alpha = h_1) \end{aligned}$$

$$\underline{v} = \underline{s} \times \underline{\dot{s}} / |\underline{s} \times \underline{\dot{s}}|$$

$$\underline{u}^+ = \underline{s} \times \underline{v} / |\underline{s}|$$

$$\cos \phi = \underline{u}^+ \cdot \underline{u}$$

$$h_2 = \{(s - h_1) \tan \rho\} \underline{u}^+$$

$$h_3 = \{r^2 - h_2^2 - (s - h_1)^2\}^{1/2} \cdot \underline{v}$$

Therefore:

$$\boxed{p = h_1 + h_2 + h_3} \quad (3.4)$$

(b) With an Ellipsoid

Equ. (3.4) can be used to approximate a solution. With the approximation we enter the set of equation (10.1):

$$(X - X_0)^2 + (Y - Y_0)^2 + (Z - Z_0)^2 = r^2$$

$$\frac{x^2 + y^2}{a^2} + \frac{z^2}{c^2} = 1$$

$$(X - X_0) i_1 + (Y - Y_0) j_1 + (Z - Z_0) k_1 = 0$$

The values of equ. (3.4) are approximated only:

$$(X), (Y), (Z),$$

$$((X) + dX - X_0)^2 + ((Y) + dY - Y_0)^2 + ((Z) + dZ - Z_0)^2 = r^2$$

$$\frac{((X) + dX)^2}{a^2} + \frac{((Y) + dY)^2}{a^2} + \frac{((Z) + dZ)^2}{c^2} = 1$$

$$((X) + dX - X_0) i_1 + ((Y) + dY - Y_0) j_1 + ((Z) + dZ - Z_0) k_1 = 0$$

$$\begin{aligned} ((X) - X_0)^2 + ((Y) - Y_0)^2 + ((Z) - Z_0)^2 - r^2 &= -2((X) - X_0)dX - 2((Y) - Y_0)dY - \\ &\quad - 2((Z) - Z_0)dZ \end{aligned}$$

$$\frac{(X^2)}{a^2} + \frac{(Y)^2}{a^2} + \frac{(Z)^2}{c^2} - 1 = -\frac{2(X)dX}{a^2} - \frac{2(Y)dY}{a^2} - \frac{2(Z)dZ}{c^2}$$

$$((X) - X_0) i_1 + ((Y) - Y_0) j_1 + ((Z) - Z_0) k_1 = -i_1 dX - j_1 dY - k_1 dZ$$

This set of equations is solved for dX, dY, dZ. New approximate solutions result from

$$(CX) = (X) + dX \dots$$

We need thus to iterate until dX, dY, dZ are negligible small.

3.5 FINDING IN AN IMAGE THE LOCATION OF AN OBJECT POINT

Given is a sensor position and a attitude with the help of sensor position vectors, \underline{s}_i , $i = 1, \dots, N$, altitude angles ϕ_i , ω_i , κ_i , or velocity vectors, $\dot{\underline{s}}_i$, $i = 1 \dots N$, The altitude angles define an imaging plane with a vector $\underline{\dot{s}}$, perpendicular to it.

We need to find a given object point P in the image. Figure 3.2. illustrates the problem.

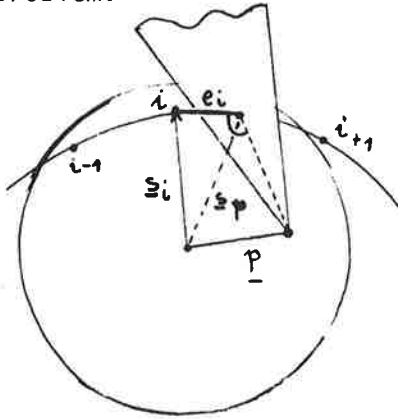


Figure 3.2: Resection with dynamic images.

We see a distance e_i :

$$e_i = \frac{\dot{\underline{s}}_i}{|\dot{\underline{s}}_i|} \cdot (\underline{s}_i - p)$$

since

$$\dot{\underline{s}}_i \cdot (\underline{s}_i - p) = |\dot{\underline{s}}_i| \cdot \underbrace{|\underline{s}_i - p|}_{e_i} \cos \alpha$$

$$\underline{s}_p = \underline{s}_i + \frac{\dot{\underline{s}}_i}{|\dot{\underline{s}}_i|} e_i$$

If $\dot{\underline{s}}_i \neq (\underline{s}_{i+1} - \underline{s}_i)$, then:

$$\underline{s}_p = \underline{s}_i + \{(\underline{s}_{i+1} - \underline{s}_i) / |\underline{s}_{i+1} - \underline{s}_i|\} \cdot e_i / \{\dot{\underline{s}}_i \cdot (\underline{s}_{i+1} - \underline{s}_i) / |\dot{\underline{s}}_i| \cdot |\underline{s}_{i+1} - \underline{s}_i|\}$$

3.6 THE USE OF A DHM FOR RECTIFICATION

We want an orthophoto / stereopartner or a simulated image.

We have a raw image, control points and a DHM, as well as a known sensor position and altitude.

We need to:

- (a) either find for each known DHM - point the corresponding image point or
- (b) find for each input image pixel the corresponding output height.

The first problem was solved in section in a resampling procedure, the DHM relates to the output image pixel. To each output pixel we need to find the input image coordinates and thus input pixels.

In the direct method, a projection ray is intersected with a plane at an assumed height (h), using procedures such as those of or

This leads to a position (X) , (Y) . But the terrain at (X) , (Y) may have height $((h))$. Thus the same is repeated with a plane at $((h))$, leading to $((X))$, $((Y))$.

We may iterate acc. to Figure 3.3:

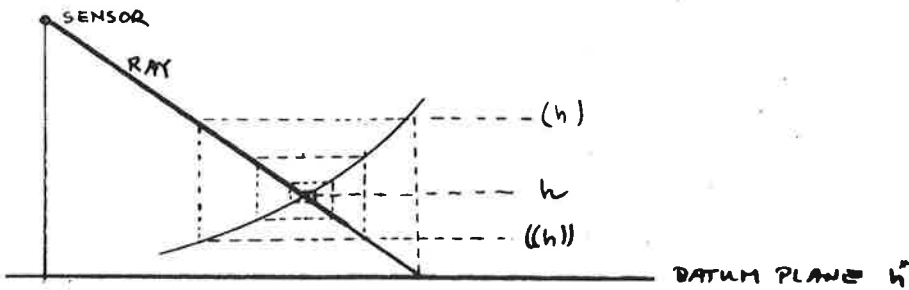


Figure 3.3: Iteration to find h .

This can now be used to create an orthophoto acc. to Figure 3.4. or a stereopartner as in Figure 3.5.

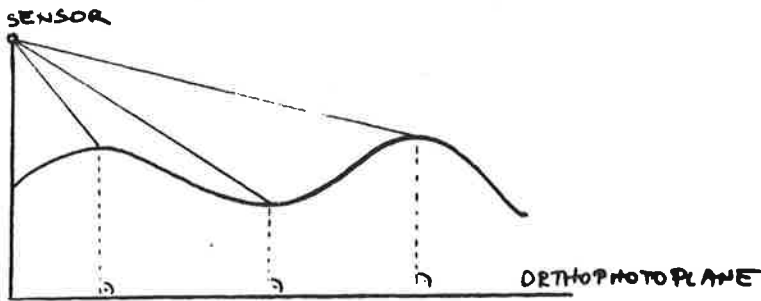


Figure 3.4: Orthophoto

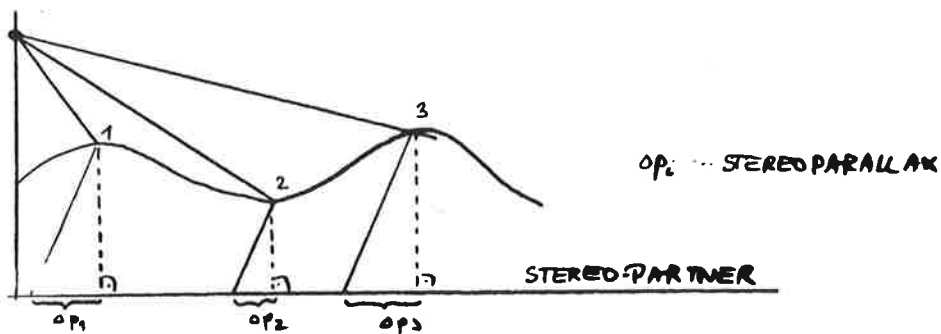


Figure 3.5: Stereopartner

With certain images, a detailed image DHM-correspondence can be helped by simulating an image from DHM. This is then used to identify homologue points in the image and the DHM-simulation image.

3.7. Stereo-scanning

See Chapter 5.2. in P1 lecture notes. So far stereo scanning was not really available. First practical work will be available with SPOT in parallel flight lines. Other concept with consequent systems exist in theory only.

3.8. Stereo-radar

a. General

See chapter 5.3 in P1 lecture notes. The main issue today is "viewability", vertical exaggeration and future satellite systems.

Current research serves to study viewability using simulated images.

Conclusions are that:

- a. same-side stereo is usually viewable. Best vertical exaggeration is with steep look angles, e.g. 10° to 20° off-nadir, and a mere 10° intersection angle.
- b. maximum same-side intersection angles are about 60° .
- c. crossing flight line stereo is feasible with intersection angles of up to 42° .
- d. Squint angles of 30° or less are acceptable for viewing in stereo.

Attached are a few illustrations on stereo-radar, including a concept for image simulation (Figures 3.6 - 3.7).

b. Stereo-formula

Parallax equations can be defined for radar.

General formulations for radar stereo computations have been proposed by Gracie et al. (1970) and others. The literature was reviewed by Leberl (1979). Simplified formulations for parallel flight lines are more commonly employed. For these recti-linear flights at constant altitude are assumed with the flight direction parallel to the object x-coordinate axis (Figure 3.6).

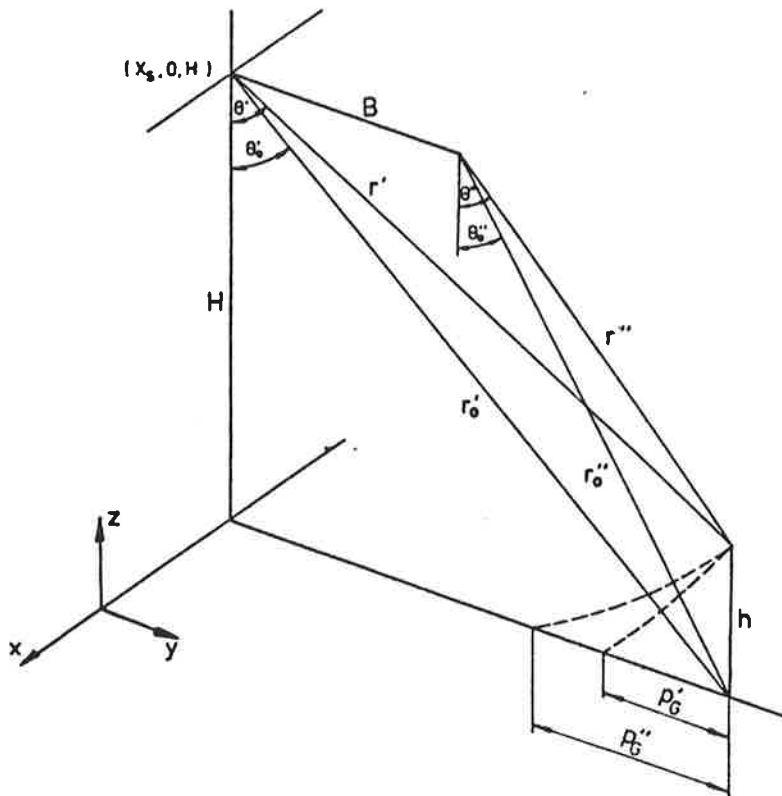


Figure 3.6.: Definition of entities for radar stereo computations.

We read from the figure that the object x_p, y_p, z_p - coordinates of a point P are:

$$\begin{aligned}x_p &= x_s && (\\y_p &= (r'^2 - r''^2 + B^2)/(2B) \\z_p &= H - ((r'^2 - y_p^2)^{1/2} + (r''^2 - (B-y_p)^2)^{1/2})/2\end{aligned}$$

where B is the stereo base, H is the flying height.

A slightly different approach to compute the height h above a reference datum is still with projection circles:

$$\begin{aligned}y &= \tan \theta' (H-h) \\y &= \pm \tan \theta'' \cdot (H-h) + B && (2.23) \\h &= H - B / (\tan \theta' \pm \tan \theta'')\end{aligned}$$

To relate the object height h above a reference datum to parallax difference d_p measured on an image pair for given look and intersection angles, we have from Figure for ground range images:

$$\begin{aligned}p_g' &= H \cot \theta_o' - H \cot \theta' \\p_g'' &= H \cot \theta_o'' - H \cot \theta''\end{aligned}$$

and

$$\begin{aligned}\cot \theta_o' &= \cot \theta' (H-h)/H \\ \cot \theta_o'' &= \cot \theta'' (H-h)/H\end{aligned}$$

combining:

$$\begin{aligned}dpg &= p_g'' - p_g' \\dpg/h &= \cot \theta' - \cot \theta'' && (2)\end{aligned}$$

Note that a given parallax dpg generates a different height h depending on θ_o' and θ_o'' . This means that apparent heights will change across a stereo model, in contrast to photographic stereo where a given parallax always corresponds to the same height independent of where in the

stereo model it has been measured.

For slant range images parallax can be defined as follows:

$$\begin{aligned} dps &= r'' - r' \\ &= (H-h) (\sec \theta'' - \sec \theta') \end{aligned} \quad (2.5)$$

Here, unlike ground range pairs, we find that zero heights still generate non-zero parallaxes. This means that the datum surface in a slant range pair will appear curved, which we may calculate by setting $h=0$, $\theta' = \theta_0'$ and $\theta'' = \theta_0''$:

$$dp_{datum} = H(\sec \theta_0'' - \sec \theta_0')$$

Topographic relief will appear to lie on top of this curved surface, according to

$$\begin{aligned} dps - dp_{datum} &= (H-h) (\sec \theta'' - \sec \theta') \\ &\quad - H(\sec \theta_0'' - \sec \theta_0') \end{aligned} \quad (2.6)$$

We also know from the geometry that

$$\begin{aligned} \tan \theta' &= y/(H-h), & \tan \theta'' &= (y-B)/(H-h), \\ \tan \theta_0' &= y/H, & \tan \theta_0'' &= (y-B)/H. \end{aligned}$$

These combine to yield

$$\begin{aligned} \sec \theta' &= (1 + \tan^2 \theta' \cdot H^2 / (H-h)^2)^{1/2} \\ \sec \theta'' &= (1 + \tan^2 \theta'' \cdot H^2 / (H-h)^2)^{1/2} \end{aligned}$$

Substituting in equ. (2.6):

$$\begin{aligned} (dps - dp_{datum})/h &= \\ &= ((H-h)^2 + H^2 \tan^2 \theta'')^{1/2} - ((H-h)^2 + H^2 \tan^2 \theta_0')^{1/2} - \\ &= H \cdot (\sec \theta_0'' - \sec \theta_0') / h \end{aligned} \quad (2.6)$$

(c) Vertical exaggeration

Radar stereo viewing conditions can be judged by a vertical exaggeration factor (Fig. 3.7).

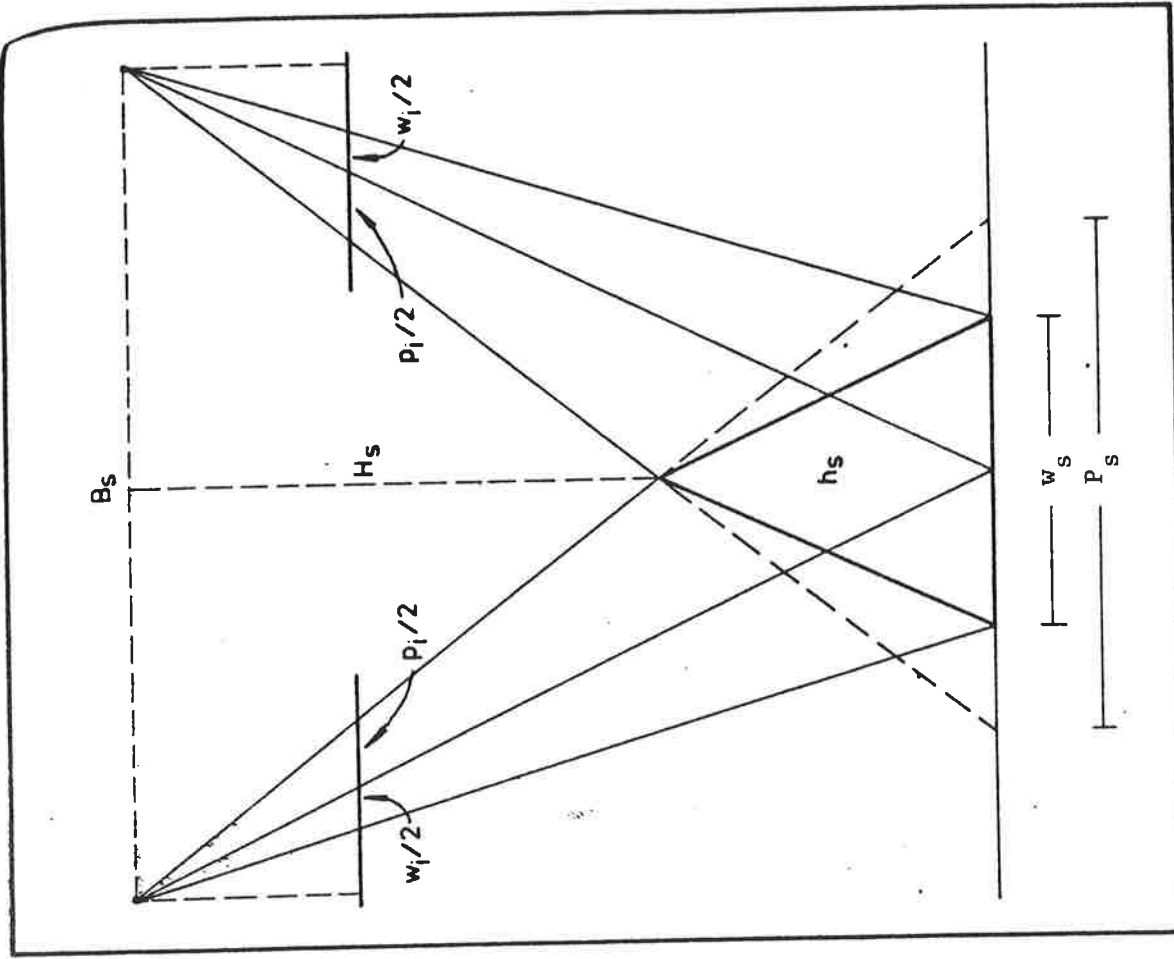


Figure 3.7.a: Definitions for the vertical exaggeration factor after La Parade et al. (1980). Object space.

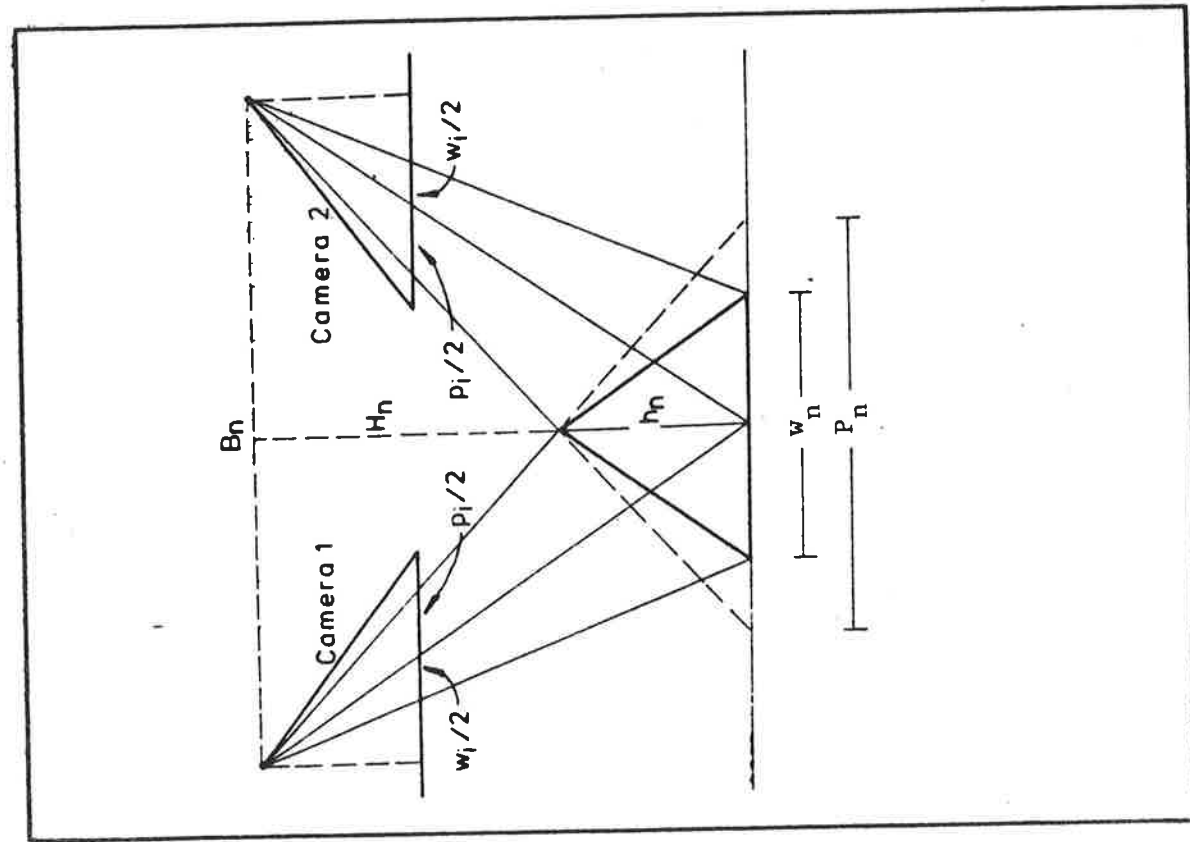


Figure 3.7.b: Definitions for the vertical exaggeration factor after La Parade et al. (1980). Stereoscopic reconstruction.

(d) Evaluation by means of simulation

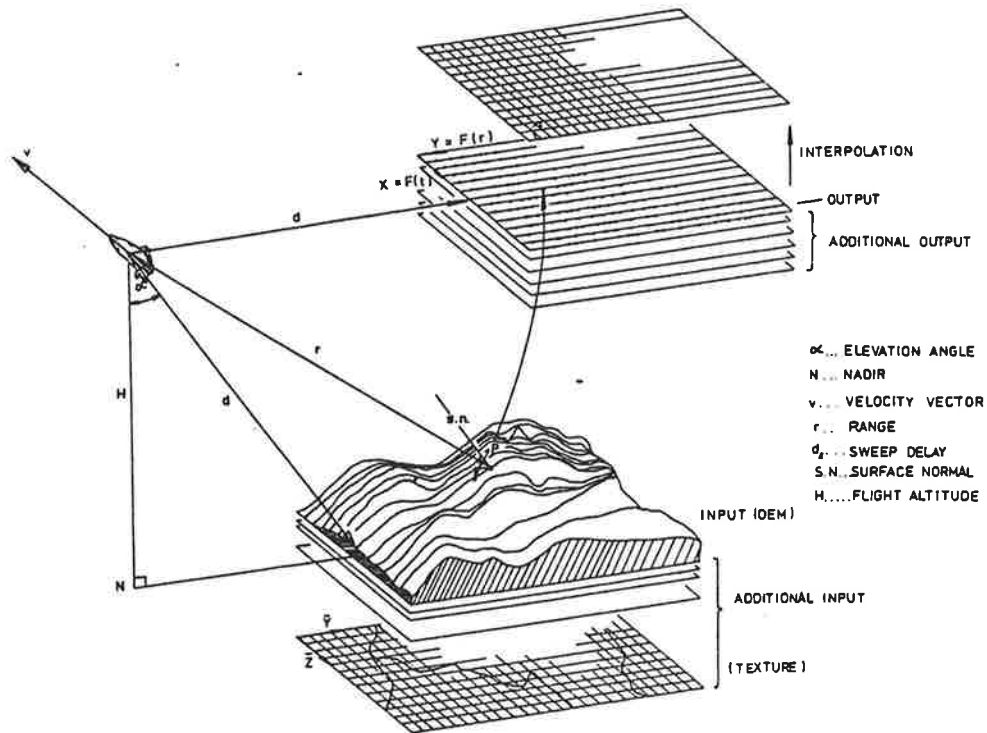
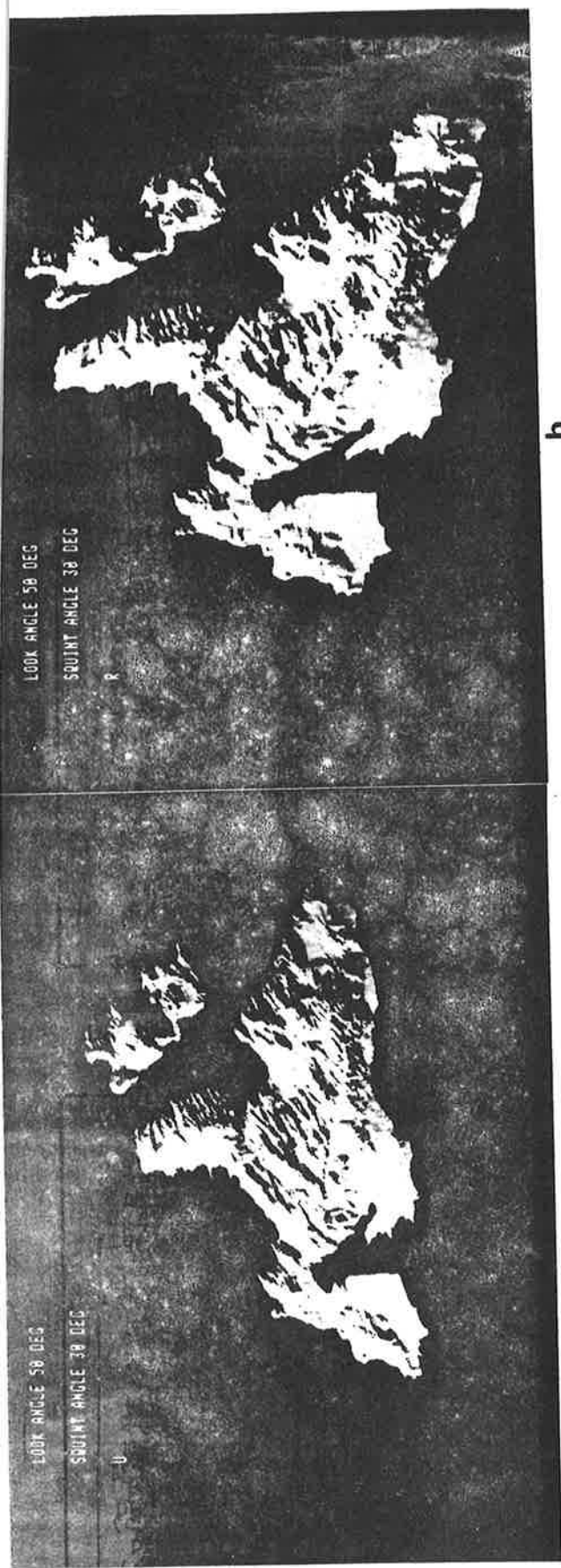


Figure 3.8: Set-up for an object space algorithm: imaging is in a plane perpendicular to the flight path (denoted by the velocity vector \underline{v}). The output values are converted to regularly spaced image points.

Image simulation can help to understand stereo-radar.
Figure 3.8. illustrates the simulation concept.



a

b

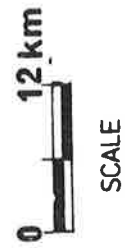
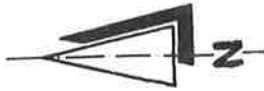
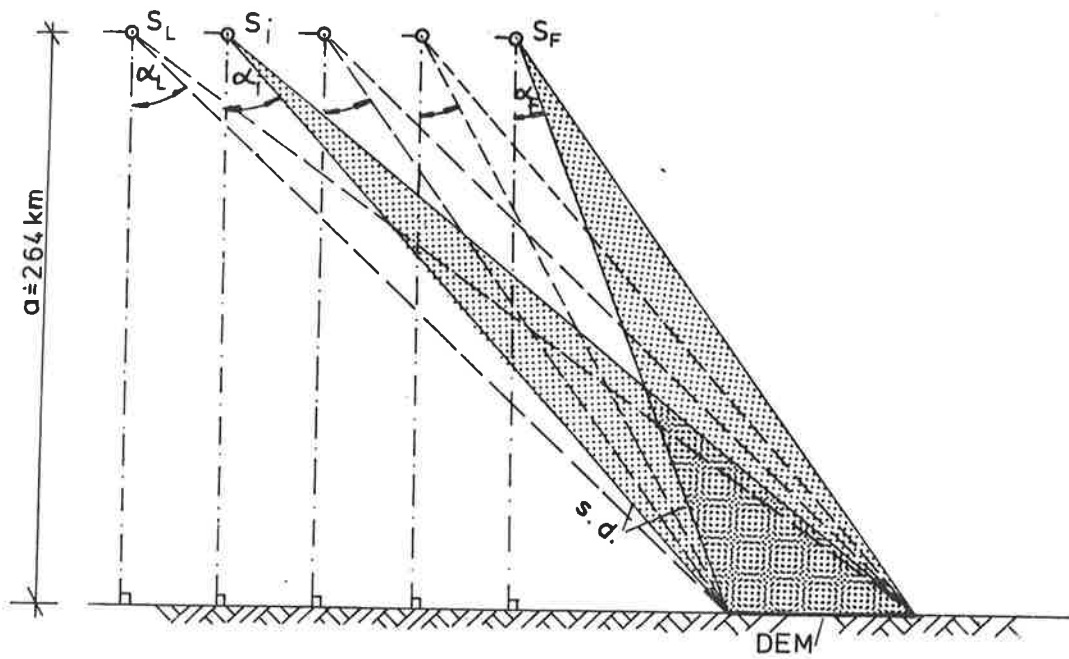


Figure 3.9: Examples of simulated radar images of the island Cephalonia (Greece), using Space Shuttle Imaging Radar (SIR-A) configurations.



- DEM Digital Elevation Model
- S_F Satellite at first flight
- S_L Satellite at last flight
- a Altitude
- s.d. Sweep Delay
- α Elevation Angle
- α_F 10°
- α_L 80°

Figure 3.10: Configurations of same side stereo.

Same Side Stereo

Look Angle	10°	15°	20°	30°	40°	47°	50°	60°	65°	70°	75°	80°
10°												
15°	6/g											
20°	5/g	7/g										
30°	3/g	8/g	8/g									
40°	1.5/m	5/g	7/g	9/g								
47°	1/n	2/g	6/g	9/g	8/g							
50°	1/n	1/g	5/g	8/g	9/g	4/g						
60°	1/n	1/n	4/g	7/g	9.5/g	7/g	7.5/g					
65°	1/n	1/n	2/g	6/g	8/g	8/g	9/g	6/g				
70°	1/n	1/n	1.5/g	5/g	8/g	9/g	10/g	7/g	7/g			
75°	1/n	1/n	1/g	3/g	8/g	7.5/g	9.5/g	8/g	8/g	7/g		
80°	1/n	1/n	1/m	2/m-g	4/g	5/g	5.5/g	5/g	4/g	4/g	5/g	

Table. 3.1 : Same side stereo evaluation.

(e) Crossing flight line stereo

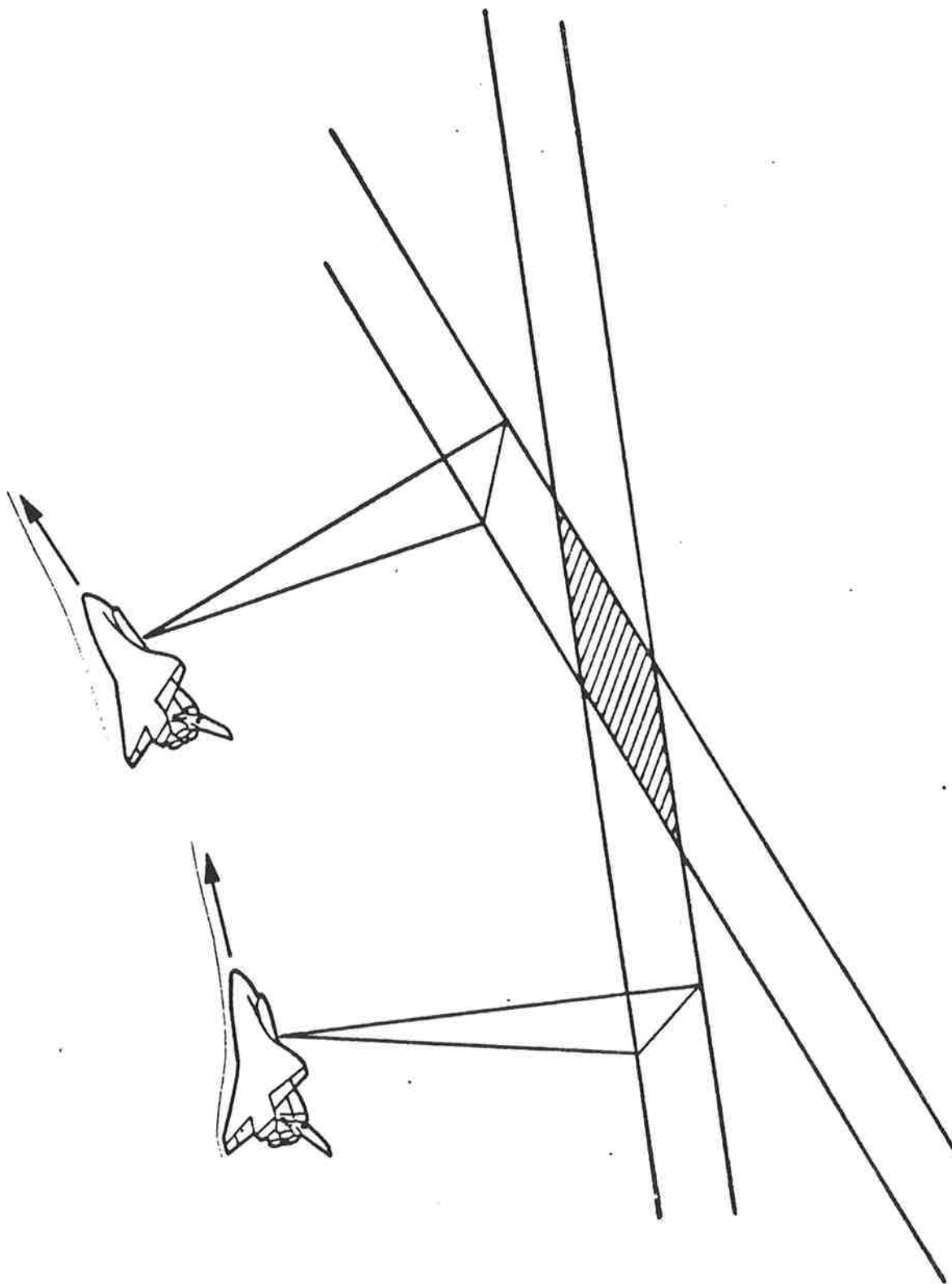


Figure 3.11.-: Sketch of the imaging geometry for SIR-A convergent stereo.

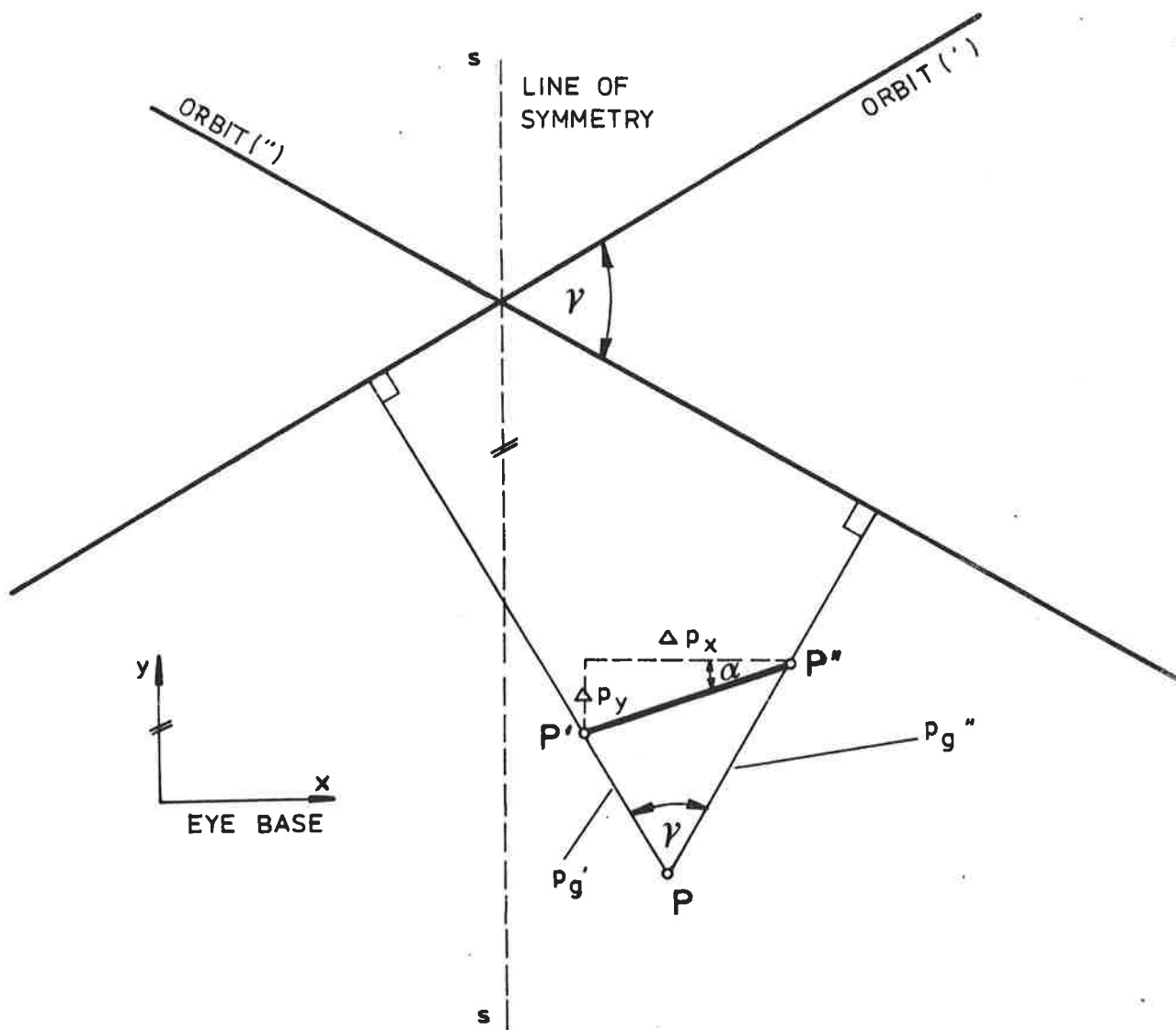


Figure 3.12: Explanation of radar stereo parallax. Ground range presentation.

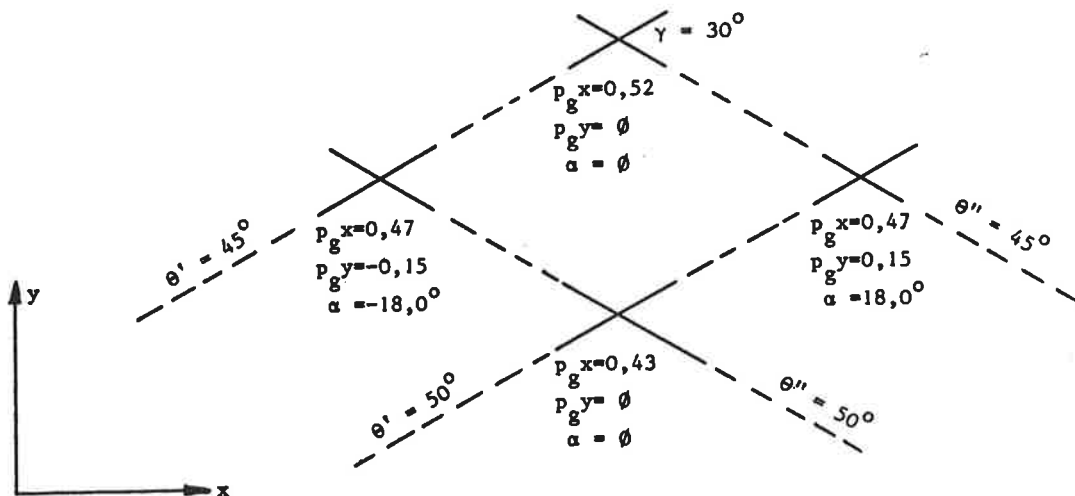


Figure 3.13: Values for parallaxes and rotation of eye base due to 1 km terrain height in the SIR-A Cephalonia stereo model.

4.1. Geometric transformations in digital image processing

(a) Introduction, Definitions

Geometric transformations of digital images are used to convert an input image into an output image of different geometry and possibly also different resolution. Simple transformations are rotation, scaling, mirror reversion, shifting. More complex ones are warping, perspective transformation etc.

These transformations are important in several cases:

- (a) to relate an image to a map or other knowledge base;
- (b) to relate one image to another in a multi-spectral, multi-spatial, multi-temporal and multi-sensor context;
- (c) to combine images of various object segments into a larger coverage in the form of mosaics.

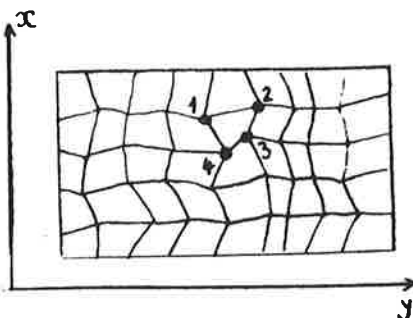
We obtain from a geometric transformation one or several of the following:

- (a) an ortho-image;
- (b) stereo partners for an ortho-image;
- (c) an image base for an information system;
- (d) stereo-parallaxes for shape-measurements (3rd dimension), (height);
- (e) the location in an image that belongs to a specific object space position and vice versa;
- (f) previously unknown or poorly known parameters of the imaging configuration (sensor exterior orientations position, attitude, sensor interior orientation);

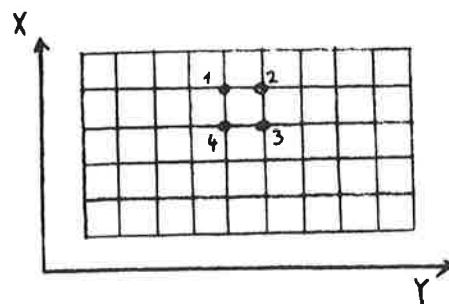
In its standard form the geometric transformation is a process that consists of two main elements:

- (a) the definition of deformations of the input image;
- (b) the creation of the output image;

This is illustrated in Figs. 4.1.



(a) Input image (deformed)



(b) output image (transformed)

Figure 4.1: (a) Geometrically deformed input image; (b) transformed output image.

Fig. 4.2 illustrates the basic numerical concept.

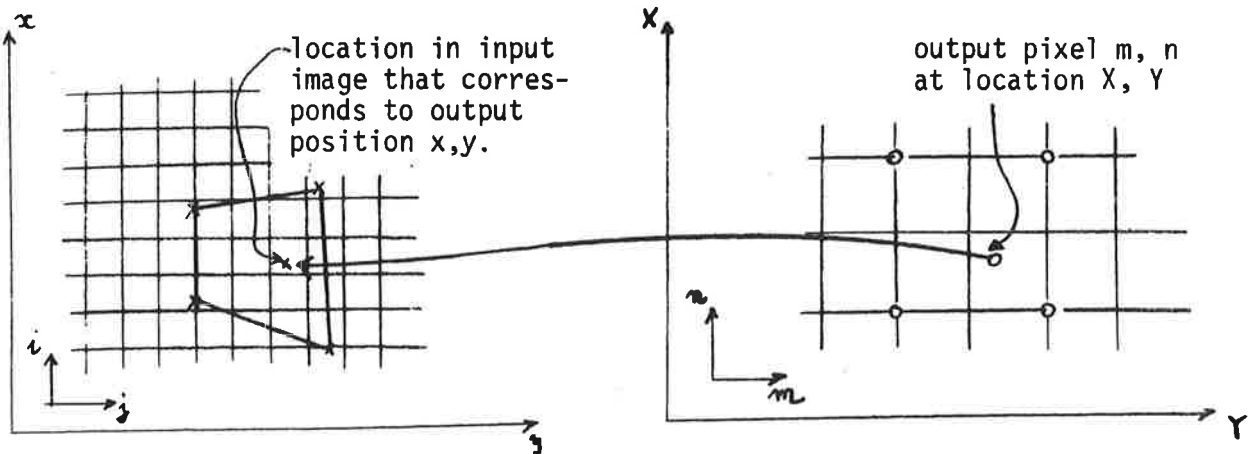


Fig. 4.2: Pixel correspondence between input and output image.

The possibly complex geometric relationship between input- and output image leads to an input position (x,y) . One can thus select the gray value encountered in that position (pixel i, j) to the output pixel (m, n) .

One calls this "resampling". In the present example one would have applied a "nearest neighbour technique" of gray value assignment. Other techniques exist as well.

An alternative to the situation in Fig. 4.2. is to proceed along input pixels (i,j) and to compute output positions (X, Y) . The gray value of the pixel (i,j) is assigned to the nearest output pixel (m, n) at position (X,Y) . This "direct method" is simpler, but has the drawback that certain output pixels remain empty, others obtain 2 assignments (Fig. 4.3). A post-processing step is required to remedy these problem.

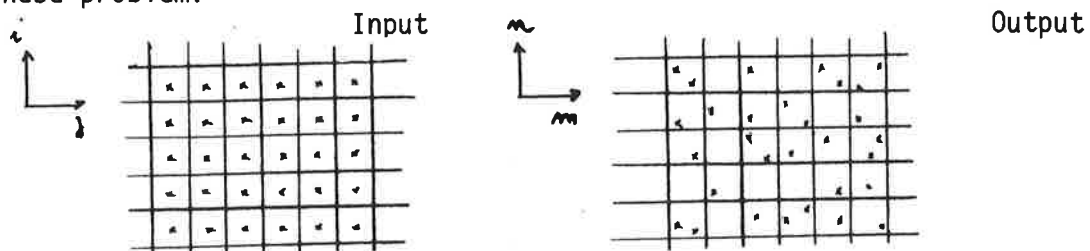


Fig. 4.3: Direct method of geometric transformation.

(b) Basic Process

(h) General

For the geometric transformation we will have to find for each input location (x, y) a deformation vector $\Delta x, \Delta y$ so that (x, y) can be transformed to an output location (X, Y) using transformation operates T_x, T_y :

$$T_x (x + \Delta x, y + \Delta y) = X$$

$$T_y (x + \Delta x, y + \Delta y) = Y$$

The task presents itself in such a form that one defines in the output image a regular grid, possibly parallel to the output coordinate axes X, Y . This leads to grid intersections $(X_m, Y_n, m = 1, M; n = 1, \dots, N)$. We call these intersections "ANCHOR POINTS".

In the input image the homologue points are not on a regular grid. Instead these points form an irregular pattern.

We create an irregular grid. Our problem now is to associate with each output anchor point (X_m, Y_n) the corresponding input anchor point (x_m, y_n) .

Once this first problem of finding corresponding anchor points is solved, one is left with the second problem of actually converting the input-to the output image.

It is at this point that the concept of pixels and gray values enters. Normally one proceeds from the output image to the input. Thus an empty output image is obtained of $\ell_1 \cdot M \times \ell_2 \cdot N$ pixels. The gray values for each of these pixels must be taken from the input image as shown in the algorithm of Figure 4.4.

```
For  $m_1, n_1 = 1$  to  $1^M, 2^N$ 
  Begin  $m_2 = \text{Integer}(m_1 / 1)$ 
         $n_2 = \text{Integer}(n_1 / 2)$ 
         $m_3 = m_1 - m_2$ 
         $n_3 = n_1 - n_2$ 
        Call Grid mesh selection ( $m_2, n_2$ , Array of anchor points)
        Call Compute Inputposition ( $m_3, n_3$ , Array of anchor points,  $x, y$ )
        Call Read input pixels ( $x, y$ , Array of input pixels)
        Call Gray value assignment ( $x, y$ , Array of input pixels, Gray value)
        Output image ( $m_1, n_1$ ) = Gray value
  End
```

Figure 4.4.: PDL description of gray value assignment.

We may encounter differences in the two images after they have been shifted on top of one another.

There is a multitude of methods to mathematically approach the problem. What should be clear now is that we perform the following process.

- (a) we find correspondenc points (control points);
- (b) we perform a transformation of $(X,Y$ into x,y) using the control points; thereby defining the transformations T_x, T_y ;
- (c) we define deformations $\Delta x, \Delta y$ in control points in the input image;

$$\Delta x = x - T_x(x)$$

$$\Delta y = y - T_y(y)$$

- (d) we compute corresponding input image coordinates \bar{x}_a, \bar{y}_a , that correspond to output anchor points X_a, Y_a using the transformations T_x, T_y ;

$$\bar{x}_a = T_x (X_a)$$

$$\bar{y}_a = T_y (Y_a)$$

- (e) we interpolate deformations in the input anchor points, using the known deformations $\Delta x, \Delta y$ in control points:

$$x_a = \bar{x}_a + \Delta x_a = T_x (X_a) + \Delta x_a$$

$$y_a = \bar{y}_a + \Delta y_a = T_y (Y_a) + \Delta y_a$$

It should be clear now that the interpolation of deformation values and the transformation are two complementary elements in the computation of image coordinates x_a, y_a that belong to an output X_a, Y_a position.

(b) Gray Value Assignment

(i) Position

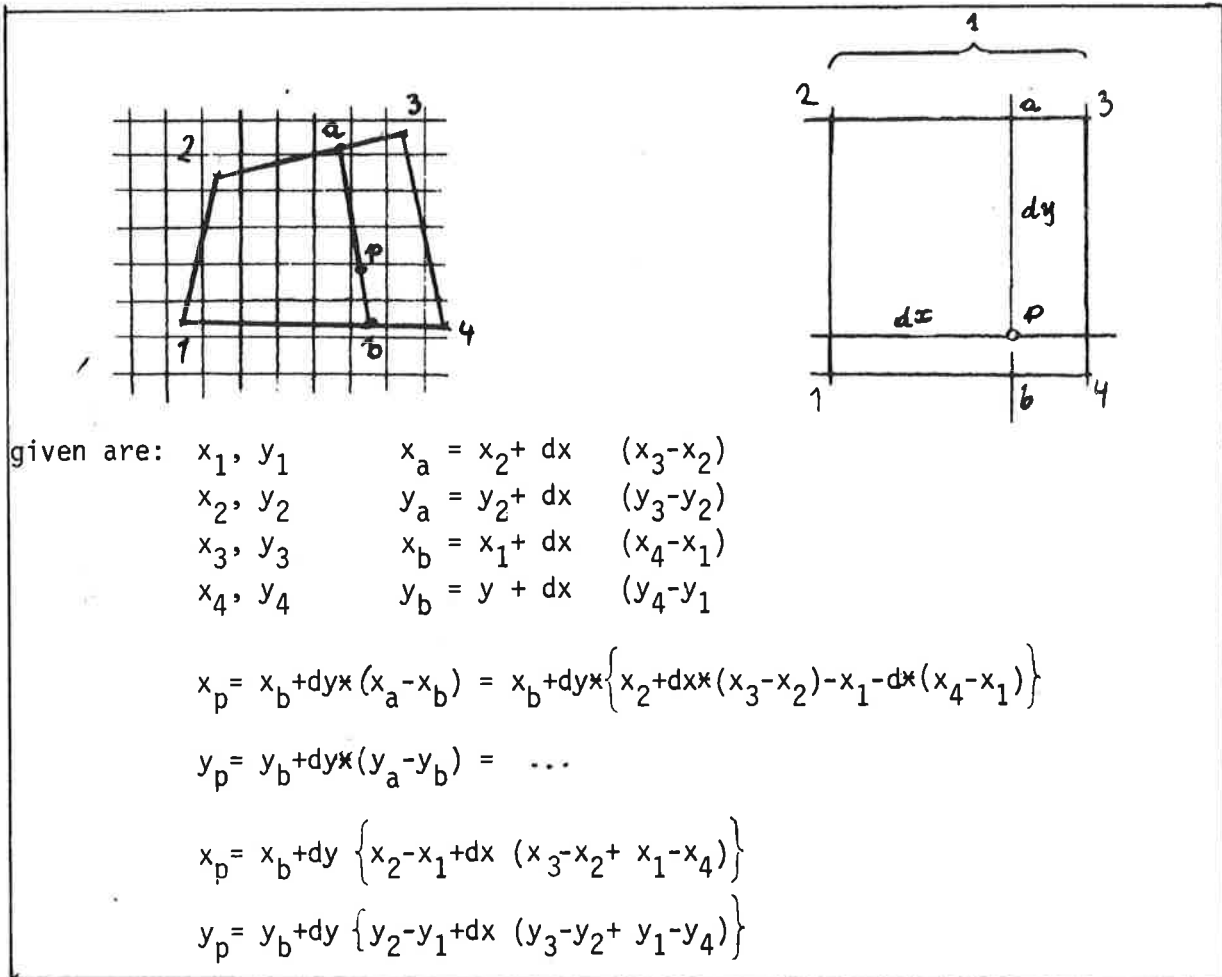
For a pixel location m, n in the output image one has to find the corresponding position in the input image. This is not with the transformation of equ. but merely with the corresponding anchor point denoted by procedure INPUT POSITION in Fig. This relies on the 4 surrounding anchor points 1, 2, 3, 4. This leads to a transformation with 4 parameters:

$$x = a_1 X + b_1 Y + c_1 XY + d_1$$

$$y = a_2 X + b_2 Y + c_2 XY + d_2$$

The output X,Y values are regular integer multiples of a grid mesh size, therefore the unknown transformation parameters $a_1 \dots d_1$, $a_2 \dots d_2$ can be computed in a simple manner. An implementation is shown in Figure 4.5.

Figure 4.5 : Interpolation in a quadrangular mesh



With the (x,y) coordinates one now has various options for gray value assignment. The nearest neighbour method has been mentioned. Others rely on the surrounding 4 (bi-linear), 9 (bi-quadratic) or 25 (bicubic) pixels of the input image. With these bi-linear methods the 4 surrounding pixels with their gray values g_1, g_2, g_3, g_4 serve as follows:

$$d_i = x - i\Delta x$$

$$d_j = y - j\Delta y$$

$$g_r = (g_4 - g_1) d_i + g_1$$

$$g_e = (g_3 - g_2) d_i + g_2$$

$$g_p = (g_e - g_r) d_j + g_r$$

This process is the above mentioned "resampling". One creates a new image with a chosen pixel size, depending on the choice of ℓ_1, ℓ_2 . Each output pixel location m_1, n_1 gets a unique gray value assignment.

The direct method is meaningful in the case of simple transformation (mirror reversion, scaling etc.) The (i,j) input pixel gray value is assigned to an output pixel by transforming (i,j) into (X, Y) . This then leads to m,n . Some double assignments and unassigned pixels may result. These problems are solved by a smoothing technique that interpolates a gray value for the unassigned pixels, using the surrounding assigned pixels. The multiple assignments are eliminated by merely accepting that particular one deriving from the nearest (X, Y) location and neglecting all other valid ones.

(j) Transformation

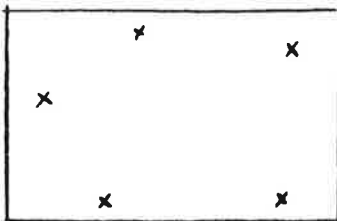
This contains two elements of interest: transformation operators T_x, T_y , and deformation vectors $(\Delta x, \Delta y)$. Both are of eminent significance to understand the entire problem.

Let us assume that we have a set of control points and a simple transformation from the x,y to the X,Y system:

$$\underline{X} \approx \lambda \underline{x} + \underline{c}_x$$

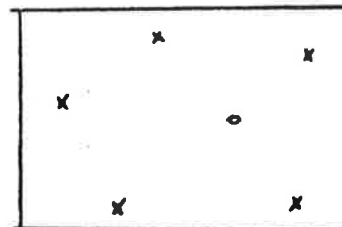
Equation (1.2) presents a scale change λ and a shift of the input image for distance c_x, c_y . However, after the shift and scaling operation the input and output positions may not match acc. to Figure 4.6.

Input image, control



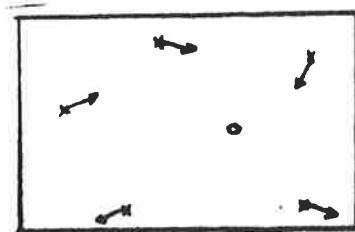
(a)

Output image, control



(b)

comparison of (a) and (b), definition of deformation



(c)

Figure 4.6: Definition of deformation after a preliminary transformation of input into output image or vice versa.

Figure 4.7. illustrates the various entities leading to equ. (2.6)

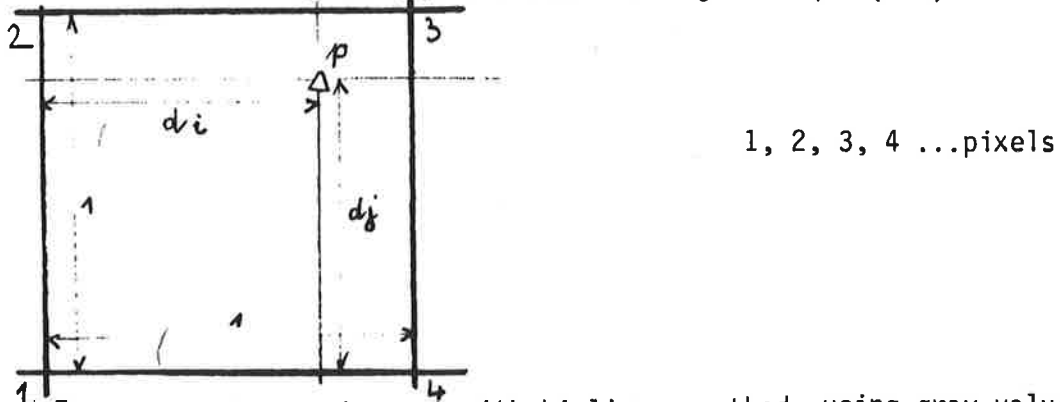


Figure 4.7.: Gray value assignment with bi-linear method, using gray values at 4 pixels 1,2,3,4 around pixel location of point p.

4.2. LANDSAT-geometry

In order to get an understanding of the image deformations in a Landsat-MSS data set one can study the individual effects of various deforming factors. This is summarized in Appendix D.

The factual presentation in App. D is quickly outdated when new types of satellite images come to bear (SPOT, TM). However, the basic concepts remain valid.

4.3. Geometric matching of two images - image registration

This is the establishment of a geometric relationship between two images with the purpose of superimposing the image onto the other so that to each pixel location we can associate the gray values in both images.

The purpose can be:

- mosaicking;
- stereo parallax measurements;
- merging two MSS images with m and u channels to an image with m + u channels;
- merging multi-temporal image for change detection.

The differences between two images are both of a geometric as well as a radiometric nature. Image registration is achieved by rectifying a "slave image" (or input-image) to conform to the "master image" (or reference image). The problem of registration is the definition of geometric differences between master and slave.

This definition of geometric differences is a well known problem in photogrammetry and probably the only area of digital image processing in which there is traditional photogrammetric activity. The topic in photogrammetry is denoted by "image correlation".

The simplest definition of geometric differences is manual measurement of homologue image details.

Automatic definition of geometric differences is based on segment-wise comparison of image-regions. In remote-sensing these regions are square or rectangular windows according to Fig.6.8. The assumption is made that geometric differences are modest so that homologue details can be found in small search areas.

The following process is now, in principle, initiated:

- (a) a small reference matrix is defined in the slave input image;
- (b) a bigger search matrix is defined in the master or reference image;
- (c) the reference matrix is placed over a location of the search matrix, centered at a particular pixel;
- (d) for this pixel of the search matrix a similarity measure is computed between the small reference matrix and the portion of the search matrix surrounding the pixel in question
- (e) the reference matrix is shifted one or several pixels and item (d) is repeated. This is carried on until (almost) all pixels of the search matrix have a similarity measure.

- (f) the maximum similarity measure is identified.
- (g) the geometric location of the maximum similarity is chosen as the location of the image point corresponding to the center of the reference matrix.

Figure 6.8 further illustrates this procedure. A reference matrix or window $W(l,m)$ with $M \times M$ pixels is defined, whereby l,m are the running indices of the pixels within the window:

$$1 \leq l,m \leq M$$

Similarly a search matrix $S(i,j)$ is defined in the input image with $L \times L$ pixels:

$$1 \leq i,j \leq L$$

whereby

$$M < L$$

For each location i,j in the search matrix, where an $M \times M$ portion is extracted from S and denoted by $S_M^{i,j}$:

$$S_M^{i,j}(l,m) \equiv S(i+l-1, j+m-1)$$

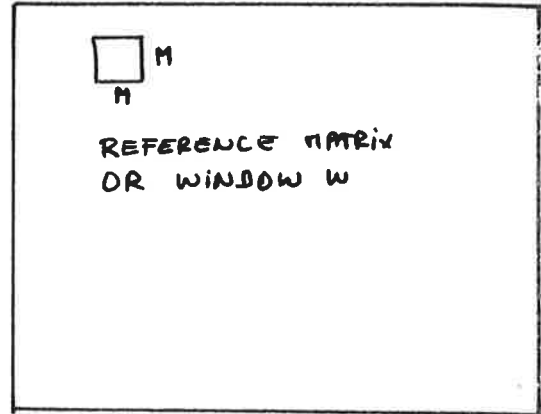
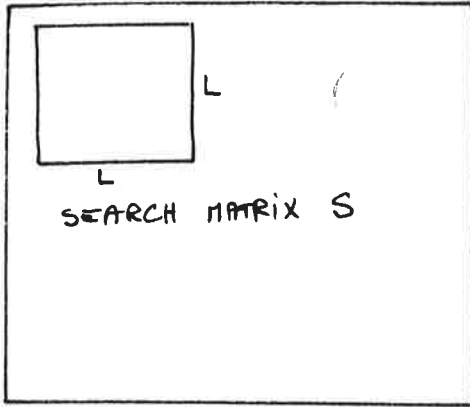
whereby l,m are again the running indices of the pixels in $S_M^{i,j}$:

$$1 \leq l,m \leq M$$

$$1 \leq i,j \leq L - M + 1$$

We now have that portion of the ~~search area~~ that we need to compute a similarity measure with W .

We now compute a measure of similarity. Often this is a cross-correlation coefficient R :



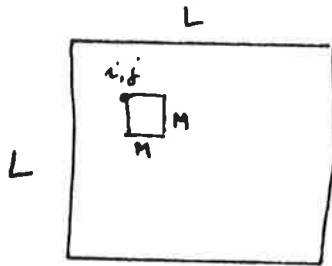
$$L > M$$

$$1 \leq i, j \leq L$$

$$S(i, j)$$

$$1 \leq l, m \leq M$$

$$W(l, m)$$



(i, j) LEFT UPPER CORNER

WE DEFINE A SUB-IMAGE OF
CALL IT:

$$S_M^{i,j}(l, m) \equiv S(i+l-1, j+m)$$

$$1 \leq l, m \leq M$$

$$1 \leq i, j \leq L - M + 1$$

Figure 4.8: Image correlation with a correlation measure.

$$R^2(i,j) = \frac{\left\{ \sum_{l=1}^M \sum_{m=1}^M W(l,m) \cdot S_M^{i,j}(l,m) \right\}^2}{\left\{ \sum_{l=1}^M \sum_{m=1}^M W^2(l,m) \right\} \left\{ \sum_{l=1}^M \sum_{m=1}^M S_M^{2i,j}(l,m) \right\}} \quad (4.1)$$

where

$$1 \leq i, j \leq L - M + 1$$

This is an expensive brute-force approach. We compute all $R^2(i,j)$ values and then look for the maximum at location i^*, j^* : This is then the homologue location.

It has been established by Anuta (1970) that the nominator of the ratio can be computed in a special fast computation device, called Fast Fourier Transform. This reduces the effort to a reasonable level.

Having a more reasonable method may even be the computation of another similarity measure, and to do this with a clever strategy of shifting the reference window W over the search matrix S . A popular measure is the one of Barnea and Silverman (1972), based on gray value differences d :

$$d(i,j;l_n,m_n) = |S_M^{i,j}(l_n,m_n) - W(l_n,m_n)| \quad (4.2)$$

where index "n" is a random sequence of integers. Instead of summing up all $M \times M$ values per (i,j) one only sums up several values:

$$I(i,j) = \left\{ r \mid \sum_{n=1}^r d(i,j,l_n,m_n) < T \right\} \quad (4.3)$$

whereby

$$1 \leq r \leq M^2$$

I is an integer number indicating how many differences were summed up until a threshold T was passed. We therefore do not go on for a location i, j with summing up large differences -- obviously we do not have homologue areas if T is exceeded after only a few differences that are summed up. The homologue point is that with the largest value for I. This algorithm is famous under the name SSDA (Sequential Similarity Detection Algorithm).

Both algorithms, equs. (4.2) and (4.3) do not consider geometric constraints between two images, such as those available in metric photography. Here we know that homologue image points are on corresponding epi-polar lines. This greatly simplifies the computational efforts since it permits one-dimensional searches for maximum correspondence. However, epi-polar line correlation is pure photogrammetry and therefore not treated here.

We do have difficulties in the similarity detection with gray tone differences in two images, due to different contrast manipulation, sun-angles, or perhaps different sensors (think of correlating an image with a synthetic image created from a DTM). We also have difficulties with geometric differences within a reference matrix W and search matrix S_M^i, j and we have finally problems with image rotations and scale differences.

5. DISCUSSION OF FUTURE SATELLITES

At ITC, S. Hempenius has compiled a collection of arguments regarding future remote sensing satellite systems.

The result is presented as an ITC-Journal paper (1983/1).

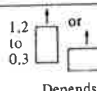
The core-table is enclosed and is self-explanatory.

We see that:

- (a) there is not a great number of future satellites; essentially one has Landsat 4/5 and SPOT. Other systems are only on the drawing board.
- (b) there is no proliferation of high spectral resolution but only an increase in geometrical resolution.
- (c) stereo is of increasing concern.

Second generation satellites

TABLE 1 Satellite specifications

TECHNICAL SPECIFICATIONS	LANDSAT-4 NASA/NOAA	SPOT CNES	TERS LAPAN/NIVR	MAPSAT Itek/USGS	STEREOSAT Geosat	LFC NASA/Itek	ATLAS-A/B ESA/Zeiss	ATLAS-C ESA/Zeiss
1 Launch date Nominal orbit height (km)	July 1982 705	Jan 1985 832	Late 1980s 1680	After 1986 ^a 919	After 1985 ^a 713	1984 300	1983-1987 250	Proposal 1987 500 (max) 200 (min) ^b
2 Sensor $\left\{ \begin{array}{l} \text{Name} \\ \text{Number} \end{array} \right.$ Principal distance (mm)	TM MSS 1 1(fixed)	HRV 2 (pointable)	Linear array 1 2000	Linear array 3 1190 Vertical Oblique	Linear array 3 705 Vertical 775 Oblique	Aerial camera 1 305	Aerial camera 1 305	Aerial camera 1 (Remote control) 305/610
3 Format (mm) Across track linear array length (mm)	(Scanning mirror)	72	119	230	61	230 x 460	230 x 230	230 x 230
4 View direction of optical axis Max off nadir viewing $\left\{ \begin{array}{l} \text{along track} \\ \text{across track} \end{array} \right.$ Additional off-nadir angle due to earth's curvature	Vertical 0° + 7.5° + 1°	Vertical 0° Adjustable up to $\pm 27^\circ$ + 2° ^a	Vertical 0° Adjustable up to 33.5° + 10° (max)	Fore Vert Aft 0° 23° 5.6° 23° + 1°	Fore Vert Aft 0° 24° 2.5° 24° + .25°	Nearly vertical 460 mm 230 mm 257 mm 40° + 2.5°	Nearly vertical 230 mm 163 mm 28° + 1.5°	For 610 mm 15° + .75°
5 Nominal focal plane scale Sensor element size in focal plane (μm)	N/A (Across track scanning)	13	15	13	15	Scale of exposed negative (maximum)		
6 Base to $\left\{ \begin{array}{l} \text{along track} \\ \text{across track} \end{array} \right.$ height ratio Earth curvature B/H modified	(TM and MSS) N/A ≈ 0.1 partial side overlap	1.0 (max) + 19%	N/A	0.42 Vert + Fore or Aft 0.85 Fore + Aft + 12.6%	0.44 0.88 + 10%	1.2 to 0.3 or 	0.3 to 0.6 in track Depends on overlap and ground track spacing	
7 Spatial resolution Pixel size in terrain (m) IFOV	TM MSS 35 80 30 56x79	20 (color) 14 (pan) 10 (pan) Vertical view only	20 (color) 14 (pan) 10 (pan) At equator only	10	15	5 - 8 ^a	4 - 6 ^a	3 - 5 ^a
8 Spectral resolution No. of spectral bands in Vis and NIR	TM MSS 6 bands 4 bands	Color mode 3 Pan 1	Color mode 3 Pan 1	Fore Aft Vert 3 Color	Fore Aft Vert 1 Pan 1 Pan 3 Color	1 panchromatic 3 layer	B & W Color	Film Film
9 Temporal resolution (days) Revisit capabilities in sidelap (days)	16 7.9	26 3 to 5 selective 5 to 3	(5) 1 or less N/A	18 1.17 poor	48 23,25	N/A poor		15 approx N/A
10 Cloud aspect information Complete coverage of region ^a	Indirect feedback on cloud cover 1 year 1/3 year		Real time cloud sensor 1/2 year 1 year		Indirect feed- back 3 years	No knowledge about cloud cover until complete film is recovered and developed years many years 6 months		
11 Ground coverage at sea level (km ²) Swath width at sea level (km)	185	2 x 60 indep. Out of 850 km range	100 Out of 2222 km range	180	61.4	225 x 450 450 x 225 Across track x Along track	188 x 188	152 x 152
12 Stereoscopic coverage	Somewhat in lateral overlap	Only lateral but can be complete on command	Never	Along track systematically Epipolar condition		Complete stereo coverage 50% overlap Multiple coverage with less overlap		
13 Accuracy Planimetric $\left\{ \begin{array}{l} \text{Relative (m)} \\ \text{Absolute (m)} \end{array} \right.$ Height (m) Minimum contour level	A few pixels ^a A few "pixels" (in side overlap) ^a	1 - 2 pixels 1 - 2 pixels (larger pixels) ^a 40	A few pixels (oblique viewing larger pixels) N/A	7 - 25 50 - 100 6? 20	100 - 200 25 100	15 15 15 - 30 Depends on instrumental and computational effort 10-15 15 12? 20-30		
14 Geometric/cartographic control	Rather dense network	Dense network ^a	N/A	Min control 1 point/1000 km ^a	Little ground control ^a	Minor control with triangulation/block adjustment Elliptical orbit poses problems		
15 Maximum topo- graphic map scale $\left\{ \begin{array}{l} \text{Produce} \\ \text{Renew} \end{array} \right.$	1:500 000 1:250 000 ^a	1:100 000 1:50 000 ^a	1:100 000 ^b 1:50 000 ^b	1:50 000 1:25 000 ^a	1:100 000 1:50 000 ^a	1:50 000 1:25 000		
16 Feasible scale of map substitute	Thematic 1:100 000	Thematic 1:30 000	1:50 000 often oblique	Thematic 1:25 000	Thematic 1:25 000	1:25 000		

- NOTES
- 1a Project in initial phase (only on paper)
 - 1b The only elliptical orbit
 - 4a Adjustable off-nadir viewing in across-track direction
 - 4b "Base-to-height ratio" concept modified to earth curvature
 - 7a Concept of equivalent pixel size of photo negatives is used
 - 13a Similar to planimetric accuracy, height accuracy is indicated in pixel size
 - 14a Doppler satellite positioning of terrain points could be used
 - 15a Height accuracy is most crucial in the positioned scales
 - 15b TERS lacks height data, "maps" contain planimetry only

6. THE APPLICABILITY OF SATELLITE REMOTE SENSING TO SMALL AND MEDIUM SCALE MAPPING

Franz W. Leberl

Institute for Image Processing and Computer Graphics
Technical University and Graz Research Center
A - 8010 Graz, Wastiangasse 6, AUSTRIA

ABSTRACT / RESUME

There are unclear prospects regarding the usefulness of satellite remote sensing images to the generation and updating of general purpose maps at scales 1: 50 000 to 1: 100 000. There is a world-wide need for such mapping. This paper examines space imagery of current and future projects to determine in how far it can satisfy these needs. It conventional medium and small scale mapping will simply not be satisfied by space imagery. A precondition for the applicability is the need to develop either new attitudes and value systems in the mapping world, or to generate space imagery at higher geometric resolution of about 3 m or better.

Keywords: Planimetric and topographic mapping, photogrammetry, radar imaging, scanning, space photography.

an early paper by PETRIE (1970). Currently available satellite images of LANDSAT, SEASAT and SKYLAB are proof to this claim. Currently planned satellite missions will also not be appropriate for the establishment of conventional maps.

Therefore, if space remote sensing is to significantly contribute to general purpose mapping then there must either be a change in the value system attached to maps or much higher geometric resolution imagery must be generated. Both avenues are open.

Space remote sensing so far has only been experimental. However, many studies have proposed with some optimism that space platforms will be appropriate to generate imagery sufficient for 1: 50 000 scale mapping and smaller (ITEK, 1981, COLVOCORESSES, 1981; DUCHER, 1980, SPOT, 1981, KONECNY et al., 1981). In order to obtain a clearer view of the arguments to support or discard these hopes, this paper will first review the thinking that dominates current map and image scale considerations in the map-making world. This is then contrasted with the capabilities offered by current and proposed satellite remote sensing missions.

The conclusion is then obvious that conventional general purpose mapping cannot be a "driver" for future space missions. Some significant change of attitudes in the map-making world would be required to lead to medium scale mapping applications of satellite images.

6. 1. INTRODUCTION

Medium and small scale mapping is here meant to concern general purpose maps at scales 1: 50 000 to 1: 100 000. The scales of 1: 250 000 and beyond are considered to belong to the realm of atlas cartography.

Remote sensing imagery from satellites is with microwaves (side-looking radar), with scanning or push-broom scanning, and with cameras. From aircraft we also have radar and scanning. Air - photography, however, would more appropriately be kept apart from remote sensing and called the topic of photogrammetry.

A mere 35 % of terrestrial land areas are mapped at scales 1: 100 000 and larger (Schwidersky, Ackermann, 1976, Konecny et al. 1979) or 25 % at scales 1: 50 000 and larger, and revision cycles are widely seen to be inappropriate. This clearly leads to the conclusion that some change has to occur in the ways that mapping is currently being done. The question is often raised whether satellite remote sensing is appropriate to solve this problem.

This paper makes the point that space imaging cannot be the basis of general purpose non-thematic mapping at medium and small scales in the current value system. It thus follows the view expressed in

6. 2. CURRENT MEDIUM AND SMALL SCALE MAPPING

In industrialized countries the small scale maps often derive from generalized larger scale maps. Original mapping may thus be at scale 1: 10 000 or 1: 25 000. In developing countries it is the smaller scale that is subject of direct mapping.

A certain map scale is considered to require a certain image or photo scale for satisfactory accuracy and interpretability. Regarding accuracy the standards are easily verifiable. Height and planimetric accuracy must be considered separately. Image scales are a function of flying height and type of camera.

Flying height is limited by the ceiling of a survey aircraft. The current limits towards small imaging scales are near 15 - 16 km. Special aircraft

may reach 20 km and more.

Cameras have standard formats and focal (principal) distances. For small scale photography these are principal distances of 8.5 cm (super-wide angle camera) and 15 cm (wide-angle camera), given a format of 23 x 23 cm² for the images. A resolution of 40 lp/mm is considered to be achievable. This limit results from the need for highly sensitive films to image in an environment that is poor in contrast. Geometric resolution must be combined with great accuracy and stability. The latter requirement may be relaxed in a computer-controlled and thus flexible photogrammetric mapping system when compared to more traditional analog systems.

2.1 Geometric Accuracy Considerations

(a) Height

Medium and small scale maps contain height information in the form of contour lines at height intervals, CI, of 10 to 20 m. This converts to the required height accuracy, σ_H , of measuring an individual point as follows:

$$\begin{aligned} \sigma_H / CI &\approx 1/4 \text{ to } 1/5 && \text{in Europe} \\ \sigma_H / CI &\approx 1/3 && \text{in U.S.A.} \end{aligned} \quad \dots(1)$$

A 10 to 20 m equidistance leads thus to a required accuracy σ_H of 4 to 7 m.

Converting this required value σ_H to an image scale of conventional photogrammetry, we use a rule of thumb for wide-angle cameras:

$$\sigma_H \approx 0.2\% \cdot H \quad \dots(2)$$

Thus a photogrammetric system based on wide-angle photography allows one to achieve height accuracies of 2 parts in 10 000 of the flying height. This in turn leads to image scales as follows:

$$\begin{aligned} \sigma_H = 4 \text{ m} \rightarrow H_{wa} = 20 \text{ km} \rightarrow 1:130\,000 \rightarrow H_{swa} = 11 \text{ km} \\ \sigma_H = 7 \text{ m} \rightarrow H_{wa} = 35 \text{ km} \rightarrow 1:230\,000 \rightarrow H_{swa} = 20 \text{ km} \end{aligned}$$

H_{wa} is the acceptable flying height with wide-angle cameras, H_{swa} for super wide-angle cameras. This implies an accuracy of WA- and SWA cameras that is equal at equal image scales.

(b) Planimetry

In a map one presents graphical accuracy on a printing base. The commonly accepted accuracy standard in large scale maps is 0.1 mm to 0.2 mm. However, in a small scale map one needs a considerable degree of generalisation, symbolisation and prioritizing. This in turn leads to geometric displacements in a map of up to 0.5 mm. Planimetric accuracy is thus far less stringent than height accuracy.

2.2 Considerations of Interpretability

The interpretability of images is the decision factor in judging the usefulness for medium and small scale mapping. Various rules exist that relate a map scale number, m_m , to the required image scale number m_i . According to standard photogrammetric text books, a common rule is (e.g. Schwidesfsky and Ackermann, 1976):

$$m_i \approx 250 \cdot m_m^{1/2} \quad \dots(3)$$

For ortho-photo maps, a standard, f.e. in Germany, is acc. to Hobbie (1974):

$$m_i \approx 17 \cdot m_m^{0.85} \quad \dots(4)$$

This leads to required image scales of about 1:100 000 for maps 1:50 000, and image scales of about 1:200 000 for maps 1:100 000. However, the above rules essentially apply to larger scales. At map scales 1:50 000 one often uses image that are much larger than the rules (3) and (4) would suggest.

This is justified by relaxed requirements for field completion and represents a "safety factor" to ensure that all significant details are presented in the maps.

2.3 Discussion

The comparison of the various considerations to define a required image scale for mapping reveals that interpretability is the most limiting factor. In order to define a geometric resolution figure, λ , instead of scale, and to compare aerial photography with digital remote sensing images, one needs to relate line-pairs per millimeter to pixel sizes on the ground. This can be achieved employing the well-known Kell factor or Shannon-theorem. According to these, n lp/mm are resolved by at least $2 \cdot n$, better about $2.8 \cdot n$ pixels.

This leads to the conclusion that on aerial film with 20 to 40 lp/mm resolution an equivalent pixel diameter is between 9 μ m and 25 μ m or, to take but a single value, about 17 μ m. Figure 1 presents the pixel diameter on the ground as a function of image scale. An obvious conclusion is that a 1 m resolution or better is usually considered necessary for medium to small scale mapping.

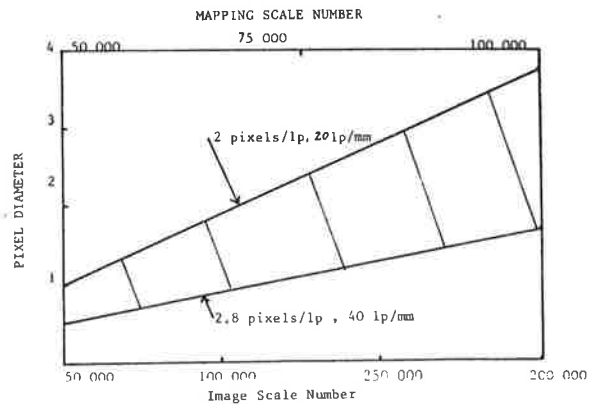


Figure 1: Required photoscale number for a given mapscale, and resulting equivalent pixel diameter on the ground.

We may thus summarize that conventional mapping standards dictate the following image performance:

- height accuracy + 5 m
- plan accuracy + 15 m
- pixel diameter 1 m

APPLICABILITY OF RS DATA TO SMALL-SCALE MAPPING

2.4 Cost of Conventional Small and Medium Scale Mapping

The cost of aerial photography is a varying entity. It tends to become more economical as the area to be covered increases. To acquire aerial photography at small scales may cost US\$ 10.--per photograph or an amount of less than US\$ 1.-- per sqkm.

In order to obtain an estimate of the cost for photogrammetric plotting one needs to know the number of stereo models required for a given area and image scale. Based on a usable stereo overlap, a stereomodel covers 8 x 10 sqcm. Therefore the effective ground coverage at scale 1: 50 000 is 40 sqkm. Table 1 presents the area per stereomodel, flying height and image scale, and number of models per 100 000 sqkm.

Image Scale Number	Ground area covered(sqkm)	Flying height (km)		Nr. of stereo models 100 000 sqkm	Man years of plotting for 100 000 sqkm
		f=15cm	f=8.5cm		
50 000	40	7.5	4.2	2 500	4 - 1)
100 000	162	15	8.5	620	1 - 2
150 000	364	22.5	12.7	300	1/5-1
200 000	648	30	17	150	1/4-1/2

Table 1: Relating image scale to ground coverage, number of stereo models and plotting effort, based on stereo models with effective stereo coverage of 9 x 18 sqcm. One stereo instrument with 2 shifts, currently not available from aircraft.

Regarding cost for plotting at small scales, current photogrammetric literature (Schwidefsky, Ackermann, 1976) reports that up to 1 to 2 stereo-models can be plotted per shift in natural, non-built-up areas on an instrument. This converts to an overall cost of US\$ 5.-- per sqkm for the preparation of a manuscript. Cartographic work is not included.

We now find, at US\$ 5.-- per sqkm, the cost per equivalent image pixel with a ground resolution of 1 m to be US\$ 0.00005.

6. 3. PERFORMANCE OF REMOTE SENSING SYSTEMS

3.1 Side-Looking Radar

SEASAT-satellite side-looking radar offered a ground resolution of 25 m. From aircraft common resolutions are 10 m with a mapping system such as that of Goodyear-Aerospace. Higher resolutions of up to 3 m are available to civilian users but not practicable at this time.

This resolution leads to image scales of about 1: 500 000. Geometric accuracies over large areas and without dense ground control are + 100 m and poorer.

These figures make it apparent that both the resolution and geometric accuracy may approach required accuracy levels; height does not. Inter-pretability is certainly insufficient for conventional mapping.

It has become common practice to generate special radar map series at scale 1: 250 000. This scale reflects the capabilities of radar at this time: it cannot be a replacement for aerial photography for mapping, but merely an addition with a special purpose outside that of conventional medium and small scale maps.

Many areas of the world have been mapped by radar, essentially for thematic purposes, but also

in some cases with a distinct general thematic purpose in mind. Brasil, Venezuela, Guatemala, Togo, Nižeria, Japan, Nicaragua and others have been completely covered by radar maps. Colombia, Peru, Ecuador, USA, Indonesia, Philippines, Australia and others have obtained partial coverage. At a cost of US\$ 3.-- to US\$ 15.-- per sqkm one must assume that in excess of US\$ 100 Mio. have been spent on the aquisition of these radar coverages.

The rules of conventional mapping at scale 1: 250 000 would require images with pixel diameters of about 1.5 m. The fact that merely images with up to 10 m resolution are employed with current radar maps is indicative of the fact that radar is justified by other considerations than those of conventional mapping. A distinct factor is the logistics advantage: images can be obtained when and where desired.

3.2 Satellite Scanning

LANDSAT is the only satellite series that generated significant scan-data for mapping. Other satellites are or were for meteorological purposes or of short-lived, experimental purposes (SKYLAB, HCMM).

The geometrical resolution of LANDSAT multi-spectral scanning (MSS) is currently 80 m and will improve to about 30 m. The geometric mapping accuracy in planimetry is commonly reported to be in a + 50 m range with the MSS, and in the + 12 to + 15 m range with the vidicon imagery (RBV). Height measurements have been reported with accuracies of + 700 m.

Clearly these values of resolution and accuracy are entirely unacceptable for 1: 50 000 to 1: 100 000 scale mapping. The only application to mapping is for atlas-cartography at scales 1: 500 000 to 1: 1 000 000

3.3 Space Photography

Photogrammetric authors have both dismissed (PETRIE, 1970) and proposed space photography for 1: 50 000 scale mapping (KONECNY et al., 1979). Dismissal is based on considerations of scale and resolution, height accuracies, cost and the need for film recovery. Examples for space photography were obtained in the past by SKYLAB and the SOJUZ-series. With the former, two cameras produced photography at scales 1: 1 Mio. and 1: 3 Mio., where the former had equivalent ground pixel diameters of up to 6 m.

The specific choice of cameras and emphasis of accuracy -- or lack thereof -- has led to map accuracies of only + 40 m in planimetry and + 150 m in height. Space photography could certainly be better than that. In SKYLAB the main limitation to the mapping applicability was the failure to satisfactorily resolve man-made features (Mott, 1975). The practicability of space photography is limited due to the need for film recovery and the advent of CCD-sensing cameras, where linear detector arrays may ultimately not need to be configured in areal, two-dimensional form. From the point of view of conventional mapping, a 60 cm-camera in a 600 km orbit could still produce only SKYLAB-type image resolutions. Lower orbits are feasible, but create problems for long duration due to limited orbit life-times. Long duration is needed due to weather problems.

3.4 Future Satellite Remote Sensing Missions

One expects the following missions to be available in one form or another in the future:

- LANDSAT
- SPOT
- SPACELAB
- ERS - 1
- MAPSAT/STEREOSAT

There may be other missions such as a tropical satellite for Indonesia or a Japanese land observation system etc.

None of these systems will offer a geometrical resolution in excess of 10 m. This automatically disqualifies the data for 1: 50 000 or 1: 100 000 conventional mapping. And this type of mapping is presented in certain cases as an important element in the application. As seen with conventional map-maker's eyes, one may expect the following:

- The planimetric accuracy, possibly also height accuracy, can be met for 1: 50 000 scales and 20 m contouring. In the MAPSAT-concept (ITEK,1981), this high height accuracy could be achieved by accurate stabilisation of the satellite. The 10 m pixel diameter of MAPSAT converts to a film resolution of 300 lp/mm in a wide-angle camera at the same altitude; consequently a higher accuracy results than one expects from film cameras in the same orbit.
- The near orthogonal projection of a push-broom CCD-image is of interest. Stereo may be helpful for interpretation.
- The ground resolution is insufficient.
- The logistics question is unclear. Effects of weather and data accessibility/sovereignty may be a limiting factor to the application of the data.

This situation must be contrasted with the cost of conventional aerial photogrammetry using new cameras, higher flying aircraft, new films, dual exposures and computer-assisted analysis methods. This alternative must be borne in mind in any evaluation of satellite remote sensing applications.

6.4. CONCLUSIONS AND OUTLOOK

The above materials indicate that conventional medium and small scale mapping in the range of 1: 50 000 to 1: 100 000 will not be served by satellite remote sensing unless:

- the cost of imagery is sufficiently low to make it competitive with small scale aircraft photography (1: 140 000);
- the ground resolution is high (3 m or better);
- there is a distinct logistics advantage of satellite image acquisition.

There is the possibility of changes in the attitudes towards maps and in the value systems of those using them; for this a view would e.g. be taken that emphasises up-to-date map contents at the expense of map accuracy and completeness. In that case satellite data will have a role to play in this application.

In the industrialized high-technology societies such changes may be provoked by the advent of digital

geo-information systems so that maps are just a tip of a digital iceberg. In that case it may be essential to have data that are up-to-date. A monitoring function for map-makers does not exist today but may emerge in the future. If it does, then an application for satellite map making would emerge with it.

In developing countries a change of attitudes toward maps may be provoked by the space technology push and the proven insufficiency of current procedures and policies. However, there are hardly any efforts made to alert those responsible for it that time and money spent on space efforts could satisfy mapping needs possibly also with conventional aerial photogrammetry.

Until such changes of attitudes take effect, satellite remote sensing will -- for conventional medium and small scale mapping -- have no application or merely one following an attitude of "anything is better than nothing if it is for free".

In conclusion, this paper is an effort to make two points. The major of the two points is to emphasize that there is a current world of conventional map-making and values attached to it. Satellite remote sensing images are not the kind of raw material to fit this world and its values.

The minor second point of this paper is to draw attention to two facts:

- (a) a change in the current value system is needed to resolve the misery of unavailable and out-of-data-maps;
- (b) a totally new task could, should and will emerge for map-makers in the area of monitoring the environment in the framework of a digital information system.

It will be in the context of these two items that satellite remote sensing images will have a lasting and meaningful rule for general purpose map making.

REFERENCES

1. COLVOCORESSES A. (1981) Feasibility of Mapsat. Presented Paper, ASP-ACSM-Annual Convention, Washington D.C., to be published in Photogrammetric Engineering and Remote Sensing.
2. DUCHER G. (1980) The SPOT-Mission. Photogrammetric Record, Vd.38, pp.27-45.
3. HOBBIIE D. (1974) "Zur Verfahrensdisposition bei differentieller Entzerrung von photogrammetrischen Luftbildern." Deutsche Geodätische Kommission, Series C, Nr.197, 187 pages.
4. ITEK (1981) Conceptual Design of an Automated Mapping Satellite System (MAPS AT). Final Report. Contract No. 14 - 08-0001-18656 for U.S. Geological Survey.
5. KONECNY G. et al. (1979). Einsatz photogrammetrische Kameras aus dem Weltraum für kartographische Anwendungen. Heft 4, Institut für Photogrammetrie und Ingenieurmessungen, Univ.Hannover.
6. LEBERL F. (1978). Zur Herstellung von Kartenunterlagen mittels Fernerkundung und Satellitenphotographie. Geowiss.Mitteilungen, Bd.13, Techn. Univ.Wien, 189 - 223.
7. MOTT P. (1975) Applications of Satellite Imagery to Small Scale Mapping. Proceedings, ASP-ACSM Fall Convention, Phoenix, Arizona, 320 - 337.

APPLICABILITY OF RS DATA TO SMALL-SCALE MAPPING

8. PETRIE G. (1970) Some Considerations Regarding Mapping from Earth Satellites. Photogrammetric Record, 6(36).
9. SCHWIDEFSKY K, F.ACKERMANN (1976) Photogrammetrie. Teubner, Stuttgart, 38 n pp.
10. SPOT (1981) SPOT-Satellite Based Remote Sensing System. Brochure issued by CNES-Toulouse.

APPENDIX A

A. TRANSFORMATION METHODS OF DEFORMATION COMPUTATIONS

An input image is considered to be a (deformed) map. A relationship is established between input image and output coordinates through transformation and interpolation.

A.1 Linear conformal transformation

The output $X_c Y_c$ - coordinates of control point c relate to input x, y values through:

$$x_c = \lambda \cos \alpha X_c + \lambda \sin \alpha Y_c + c_x \quad (A.1)$$

$$y_c = \lambda \sin \alpha X_c + \lambda \cos \alpha Y_c + c_y$$

This is algebraically non-linear because unknown coefficients are presented in a non linear form. We need to compute scale λ , rotation α , shifts c_x, c_y or 4 substitute parameters a, b, c, d , so that we obtain a numerically linear formulation:

$$x_c = aX_c + bY_c + d \quad (A.2)$$

$$y_c = -bX_c + aY_c + c_y$$

This is a linear transformation. It is also conformal.: angles remain unchanged. We need 2 points to compute 4 unknowns a, b, c, d . This leads to 4 equations. However, we usually will have more than 4 points:

$$\begin{aligned} x_1 &= X_{c_1} a + Y_{c_1} b + c_x + 0 \cdot c_y \\ y_1 &= Y_{c_1} a - X_{c_1} b + 0 \cdot c_x + 1 \cdot c_y \\ x_2 &= X_{c_2} a + Y_{c_2} b + c_x + 0 \cdot c_y \\ y_2 &= Y_{c_2} a - X_{c_2} b + 0 \cdot c_x + 1 \cdot c_y \end{aligned} \quad (A.3)$$

$$\begin{aligned}
 x_3 &= X_{c3}a + Y_{c3}b + c_x + 0.c_y \\
 y_3 &= Y_{c3}a - X_{c3}b + 0.c_x + c_y \\
 &\vdots \\
 x_n &= X_{cn}a + Y_{cn}b + c_x + 0.c_y \\
 y_n &= Y_{cn}a - X_{cn}b + 0.c_x + c_y
 \end{aligned}
 \tag{A.3}$$

This is usually rewritten as follows:

$$\underline{\ell} = \underline{A} \underline{u}^T
 \tag{A.4}$$

where \underline{A} is a coefficient matrix, $\underline{u} = (a,b,c,d)$ is a vector of unknowns of observations. A solution is needed for \underline{u} . But one cannot invert \underline{A} because it is rectangular. The rules of least squares adjustment lead to the following:

$$\begin{aligned}
 \underline{A}^T \underline{P} \underline{\ell} &= \underline{A}^T \underline{P} \underline{A} \underline{u}^T \\
 \underline{u}^T &= (\underline{A}^T \underline{P} \underline{A})^{-1} \underline{A}^T \underline{P} \underline{\ell}
 \end{aligned}
 \tag{A.5}$$

where \underline{u} is the vector of unknowns minimizing the errors of observation, \underline{P} is a matrix of weights. We find:

$$\underline{v} = \underline{A} \underline{u} - \underline{\ell}
 \tag{A.6}$$

and

$$m_0^2 = \frac{\underline{v}^T \underline{v}}{r}
 \tag{A.7}$$

where m_0 is the mean error of a single observed image point coordinate. The values v are "residuals" in the control points. They should be random in size and direction. However, they usually form a systematic pattern. This is evidence to the fact that the image was deformed such that a linear conformal model simply is unsuitable to describe the required transformation completely.

A.2 Affine transformation

If the image is actually deformed and not merely shifted, rotated and scaled, then one has to employ transformations of a higher order. A slightly more flexible transformation is with two different scales λ_x, λ_y and a separate rotation for each coordinate axis α_x, α_y :

$$\begin{aligned}
 x &= \lambda_x \cos \alpha_x X + \lambda_y \cos \alpha_y Y + c_x \\
 y &= -\lambda_x \sin \alpha_x X + \lambda_y \cos \alpha_y Y + c_y
 \end{aligned}$$

or

$$x = aX + bY + c \tag{A.8}$$

$$y = dX + eY + f$$

This is a transformation requiring 3 control points. A triangle can always be made to fit 3 control points.

A.3 Bi-linear transformation

This is used to fit a quadrangle to 4 control points:

$$x = aX + bY + cXY + d \tag{A.9}$$

$$y = eX + fY + gXY + h$$

A.4 Higher order polynomials

One could employ higher order polynomials for the transformation:

$$x = \sum_{i=1}^I \sum_{j=1}^J a_{ij} x^{(i-1)} y^{(j-1)} \tag{A.10}$$

$$y = \sum_{m=1}^M \sum_{n=1}^N b_{ij} x^{(m-1)} y^{(n-1)}$$

with $I = J = 1$, one has the bi-linear transformation (4.8).

However, such use of polynomials generally is not very advisable due to the following problems:

- (a) polynomials with more than 10 coefficients in equ. (4.10) become unpredictable in between control points;
- (b) complex deformations cannot be well described with polynomials;
- (c) control points need to be evenly distributed;
- (d) point clusters are not of great use;
- (e) extrapolation is totally unacceptable with polynomials

Still polynomials are often used for simplicity.

A.5 Collineation

A transformation method, not interpolation, that is based on a perspective projection, uses:

$$x = \frac{a_1X + b_2Y + a_3}{c_1X + c_2Y + 1} \tag{A.11}$$

$$y = \frac{b_1X + b_2Y + b_3}{c_1X + c_2Y + 1}$$

This is a central perspective transformation between the planes XY and xy.

APPENDIX B

B.1 Arithmetic means interpolation

After an overdetermined transformation with extra control points one obtains residuals that are systematic: this means that the deformation at a point can be predicted (interpolated) from surrounding points. A simple method of interpolation or prediction is by weighted arithmetic means:

$$\Delta x_p = \frac{\sum_{i=1}^N p_i \Delta x_i}{\sum_{i=1}^N p_i} \quad (B.1)$$

$$\Delta y_p = \frac{\sum_{i=1}^N p_i \Delta y_i}{\sum_{i=1}^N p_i}$$

where p_i could be a function of distance d_i between the new point and the control point i :

$$p_i = \frac{1}{0.1 + d_i^k} \quad (B.2)$$

The constant, 0.1, is added to avoid a value of 0 to occur for $d_i = 0$. Power k can be 1/2 or 2.

computation of image coordinates x_p, y_p of a point p whose X_p, Y_p values are known, could thus be as follows:

$$\bar{x}_p = \sum_{i=1}^I \sum_{j=1}^J a_{ij} x^{i-1} y^{j-1}$$

$$\bar{y}_p = \sum_{i=1}^I \sum_{j=1}^J b_{ij} x^{i-1} y^{j-1}$$

$$x_p = \bar{x}_p + \Delta x_p$$

$$y_p = \bar{y}_p + \Delta y_p$$

(B.3)

B.2 Moving Average interpolation

The values $\Delta x_p, \Delta y_p$ in a new point p result from a polynomial of low order, say with $I=J=2$ in equ. (4.10); we compute this with just a set of selected control points around the new point (Figure B.1)

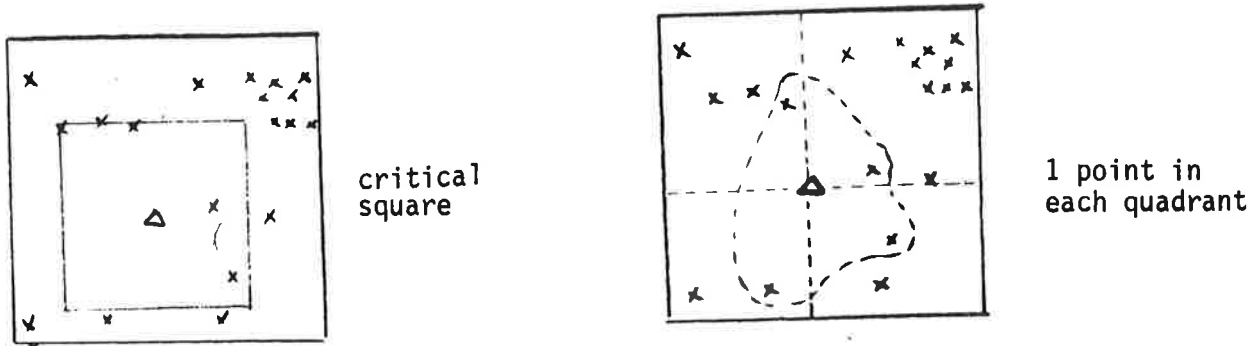


Figure B.1 : Selection of control points for moving average interpolation.

Numerical solutions follow the sequence of

- (a) selecting a control point set around new point;
- (b) reducing coordinates to new point;
- (c) computing the first coefficient of a polynomial of low order, using for each control point a weight p_i , e.g. as a function of distance d_i . Only the first coefficient is needed because \bar{X}, \bar{Y} are zero due to reduction of the coordinates to the new point.

B.3 Linear Prediction Interpolation

The x, y -discrepancies serve to define a correlation function:

$$C(d) = C_0 / (1 + d^{C_1}) \tag{B.4}$$

$$C(0) = C_2$$

where d is a correlation distance. The computation of C_0, C_1 can be with C -values that derive from

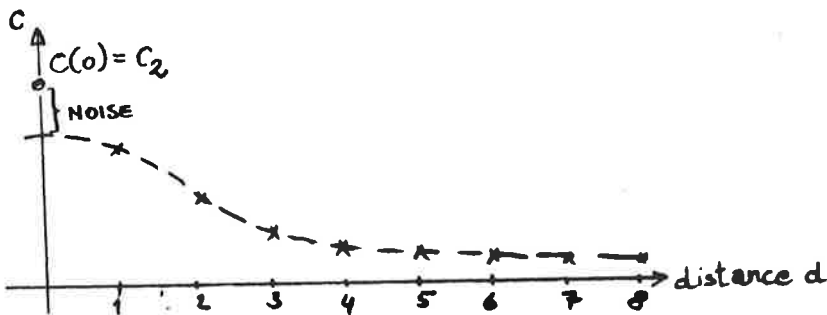


Figure B.2 : Correlation function.

given data acc. to Figure B.2. It is also common to simply assume a correlation function with a chosen set of C_0, C_1, C_2 : This is then used to compute a correlation matrix among control points:

$$\underline{C} = \begin{bmatrix} C_{11} & C_{12} & C_{13} & C_{14} \dots C_{14} \\ & C_{21} & C_{23} & C_{24} \dots C_{24} \\ & \text{symm.} & C_{33} & C_{34} \dots C_{34} \\ & & & C_{44} \dots C_{44} \\ & & & \vdots \\ & & & C_{nn} \end{bmatrix}$$

and between the new point p and the control point:

$$\underline{g}_p = \begin{bmatrix} C_{p1} \\ C_{p2} \\ C_{p3} \\ \vdots \\ C_{pn} \end{bmatrix}$$

where C_{ij} is a correlation value acc. to equ. (B.4). With this, an interpolated value x_p, y_p is obtained:

$$\Delta x_p = g_p \underline{C}^{-1} \Delta x_c \tag{B.5}$$

$$\Delta y_p = g_p \underline{C}^{-1} \Delta y_c \tag{B.6}$$

where $\Delta x_c, \Delta y_c$ is the vector of deformations in the control points.

This method is flexible in that it is robust against variable control distribution. It permits one to filter random error components by selecting a value for $d = 0$ that is larger than C_0 (compare Fig. B.2).

Moving average and linear prediction interpolation are flexible methods recommended for use.

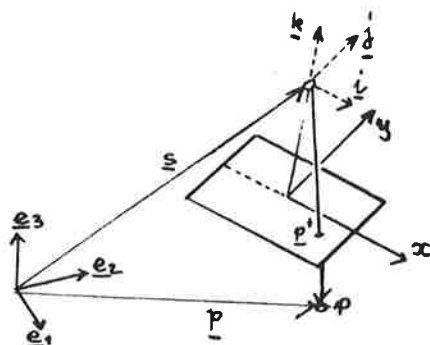
APPENDIX C

The Camera: Central Perspective

We know and are familiar with the camera central perspective:

$$\underline{p} = \begin{pmatrix} x \\ y \\ z \end{pmatrix} - \begin{pmatrix} x_0 \\ y_0 \\ z_0 \end{pmatrix} = \lambda \cdot \underline{R} \begin{pmatrix} x - x_0 \\ y - y_0 \\ -c \end{pmatrix} \tag{C.1}$$

This is illustrated by Figure 6.1



\underline{R} ... ROTATION MATRIX

$$\underline{R} = \begin{bmatrix} i_1 & j_1 & k_1 \\ i_2 & j_2 & k_2 \\ i_3 & j_3 & k_3 \end{bmatrix}$$

$$\underline{i} = (i_1, i_2, i_3) \\ = i_1 \underline{e}_1 + i_2 \underline{e}_2 + i_3 \underline{e}_3$$

Figure C.1: Central perspective.

We have:

$$\frac{x - x_0}{z - z_0} = \frac{i_1 (x - x_0) + j_1 (y - y_0) + k_1 (-c)}{i_3 (x - x_0) + j_3 (y - y_0) + k_3 (-c)} \tag{C.2}$$

$$\frac{y - y_0}{z - z_0} = \frac{i_2 (x - x_0) + j_2 (y - y_0) + k_2 (-c)}{i_3 (x - x_0) + j_3 (y - y_0) + k_3 (-c)}$$

or

$$x - x_0 = -c \frac{i_1 (x - x_0) + i_2 (y - y_0) + i_3 (z - z_0)}{k_1 (x - x_0) + k_2 (y - y_0) + k_3 (z - z_0)} \tag{C.3}$$

$$y - y_0 = -c \frac{j_1 (x - x_0) + j_2 (y - y_0) + j_3 (z - z_0)}{k_1 (x - x_0) + k_2 (y - y_0) + k_3 (z - z_0)}$$

Linearisation of equ. (C.3) leads to the following formulation, that is valid for standard vertical camera photography ($\underline{R} = \underline{E}$):

$$dx = -\frac{c}{H} dx_0 - \frac{x}{H} dz_0 + c \left(1 + \frac{x^2}{c^2}\right) d\phi - \frac{xy}{c} d\omega - y d\kappa \tag{C.4}$$

$$dy = c \frac{c}{H} dy_0 - \frac{y}{H} dz_0 - \frac{xy}{c} d\phi + c \left(1 + \frac{y^2}{c^2}\right) d\omega - x d\kappa$$

where ϕ, ω, κ are rotation angles defining matrix B. H is the flying height.

APPENDIX D

D. LANDSAT - RECTIFICATION

Historically LANDSAT image rectification systems were not based on digital image processing, but on properly controlling the film writing equipment such as the Laser-Beam Image Recorder (LBIR) or the Electron Beam Image Recorder (EBIR).

Landsat itself is assumed to be well-known. An image is formed with 6 image lines at a time in the MSS. The RBV is a TV-camera with a central perspective. We will deal with this in a later section.

The MSS is a hybrid projection: in orbit direction it is orthogonal, across orbit panoramic central perspective. We will study effects of:

- Scale deformation
- Earth curvature
- panoramic distortion
- orbit plane inclination
- Earth rotation
- (Mirror scan, non-linearity, topographic relief).

D.1 Row MSS Data

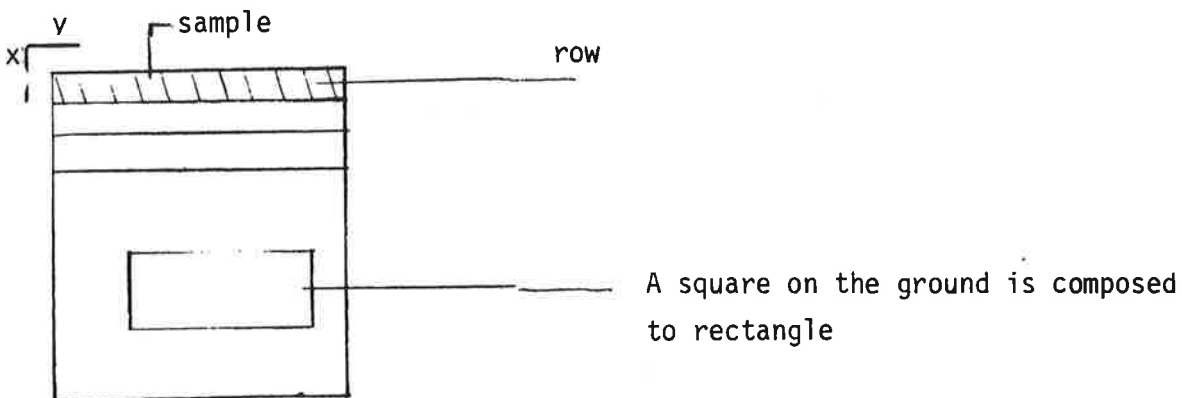


Figure D.1: Writing a LANDSAT-tape on film causes a square to appear. But this shows different scales in x, y.

D.2 Scale correction

$$\begin{Bmatrix} x' \\ y' \end{Bmatrix} = \begin{Bmatrix} S_y & 0 \\ 0 & 1 \end{Bmatrix} * \begin{Bmatrix} x \\ y \end{Bmatrix} \tag{D.1}$$

where

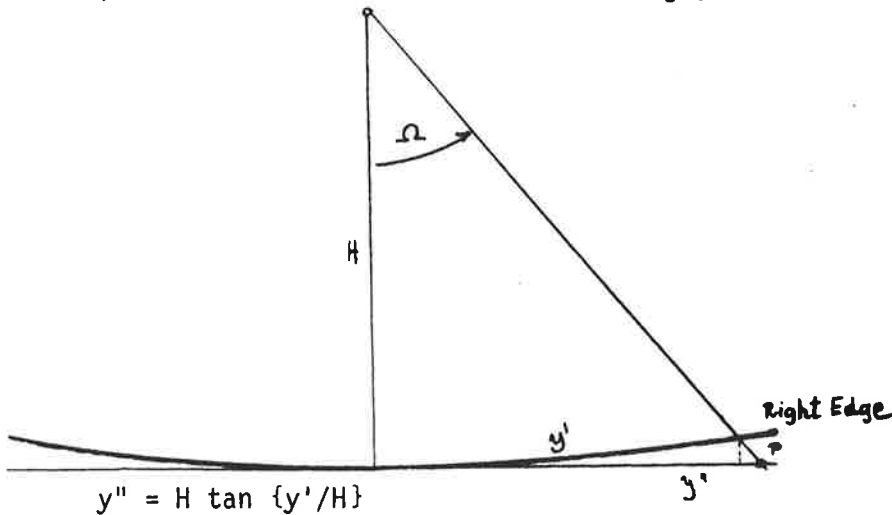
$$S_y = 79/56 = 1.4 \text{ (Dimension of the pixel on the ground is } x = 79\text{m, } y = 56\text{m).}$$

D.3 Panoramic correction and Earth curvature

Recording is with each pixel getting the same area on film. However, on the ground, each pixel covers a different area. There is both a panoramic and an earth curvature effect.

(a) Panoramic effect

A point p is at location y' in the image, when it should be at y'' (Figure 2)



(D.2.a)

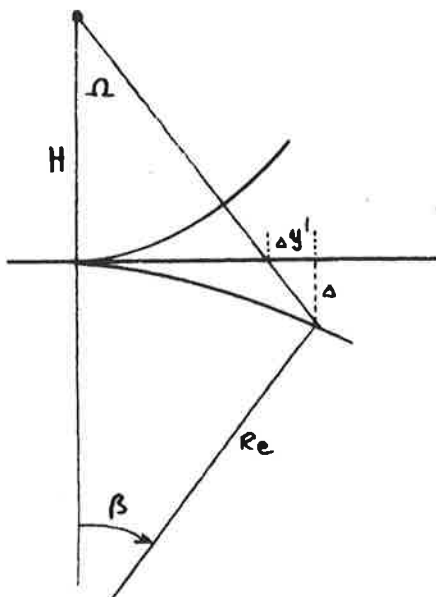
or

$$\Delta y' = H \tan \{y'/H\} - y'$$

(b) Earth curvature

Similarly, earth curvature causes a $\Delta y'$ to occur that is:

$$\Delta y' = - \frac{y''^3}{R_e 2H} \tag{D.2.b}$$



since: $\Delta \bar{y}' = - \Delta \tan \Omega$

$$\Delta = R_e - R_e \cos \beta$$

$$\Delta \approx R_e (1 - (1 - \beta^2/2))$$

$$\beta \approx \frac{H \tan \Omega}{R_e}$$

$$\Delta \approx R_e H^2 \tan^2 \Omega / (2 R_e^2)$$

$$\Delta \bar{y}' \approx -H^2 \tan^3 \Omega / 2 R_e$$

$$\Delta \bar{y}' \approx -H^2 (y''^3 / H^3) / 2 R_e$$

$$\Delta \bar{y}' \approx -y''^3 / 2 R_e H$$

Fig. D.3: Earth curvature

Fig. 5.2
Panoramic Distortion

Fig. 5.2:
Panoramic distortion

D.4 Orbit plane inclination

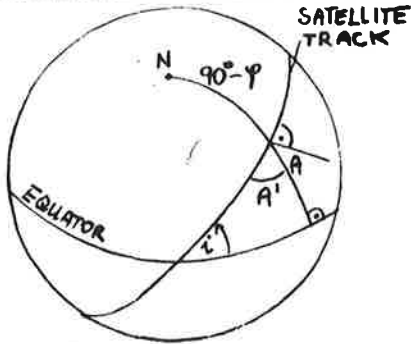


Figure D.4 a: Defining the for the effect of the orbit inclination.

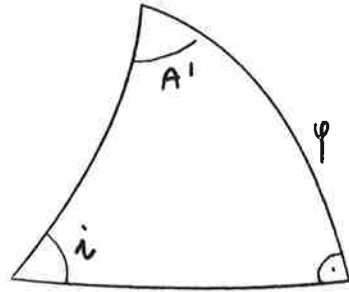


Figure D.4 b: Spherical triangle.

$$\begin{aligned} \cos i &= \cos A' \cos 90^\circ + \sin A' \sin 90^\circ \cos \phi \\ \sin A' &= + \cos i / \cos \phi \\ A &= 90^\circ - A' \\ \cos A &= + \cos i / \cos \phi \\ A &= + \cos^{-1} \{ \cos i / \cos \phi \} \end{aligned}$$

$$\begin{bmatrix} x'' \\ y'' \end{bmatrix} = \begin{bmatrix} \cos A' & \sin A' \\ -\sin A' & \cos A' \end{bmatrix} \cdot \begin{bmatrix} x' \\ y' \end{bmatrix} \tag{D.4}$$

The x-axis is pointing north, the y-axis points east.

D.5. Non linear sweep

$$\Omega = 0.29 \cdot \sin\{21.46 \times t\} \quad /t/ \leq 16.5 \text{ msec.} \longrightarrow \text{500 m effect, hardly predictable}$$

D.6 Earth Rotation - Skew

During the time of imaging, t_s , the earth is rotating towards the East under the satellite. Therefore each image point is displaced with respect to where it would be without earth rotation. This displacement is larger nearer the equator.

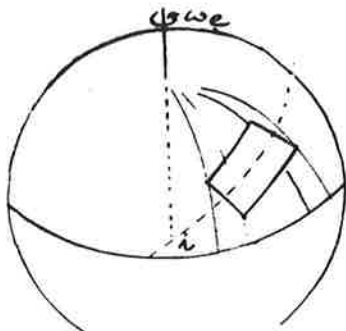


Figure D.5: Image and earth rotation

In order to quantify this effect, we state, that the velocity of the earth, v_c is:

$$v_e = R_e \cos \phi, \quad \omega_{ej} \text{ (D.4)} \quad \left| \quad \omega_e = 0.7272 \cdot 10^{-4} \text{ rad/sec.} \right.$$

The time t_s to image an image takes the length ℓ of the image divided by the satellite velocity, $R_e \cdot \omega_0$, where ω_0 is the radial velocity of the satellite:

$$t_s = \ell / (R_e \cdot \omega_0), \quad \begin{matrix} \omega_0 \approx 9.87 \cdot 10^{-4} \text{ rad/sec} \\ R_e \approx 6.37816 \cdot 10^6 \text{ m} \end{matrix} \quad \text{(D.5.)}$$

Eastward motion of image during a given time

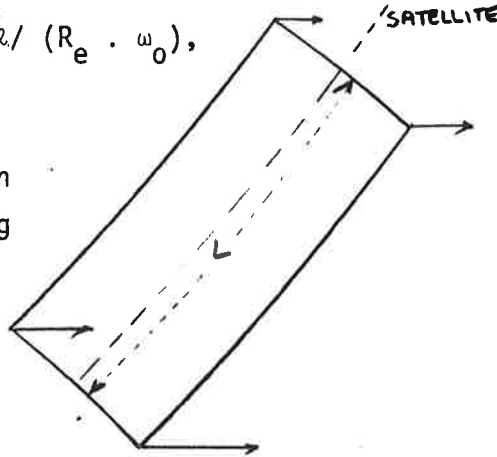


Figure D.6: Eastward motion of image corners due to Earth rotation

The actual eastward motion of the later image edge when compared with the trailing edge is:

$$\Delta y'' = t_s \cdot v_e \quad \text{(D.6)}$$

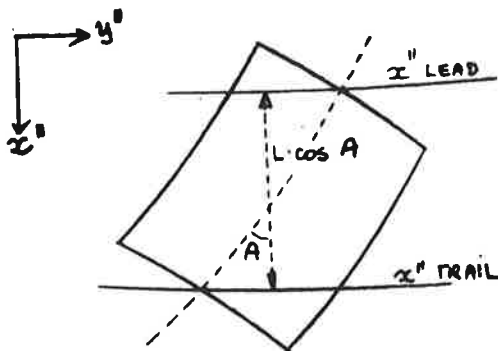
v_e at 40° latitude is 355.29 m/sec.

t_s for a 161 km frame is $161\,000 / \{6.3786 \times 10^7 \times 987 \times 10^{-4}\} = 25.5 \text{ sec}$

We thus have to shift the y'' -coordinates according to (D.6). We need to relate $t_s \cdot v_e$ to image x'' , y'' -coordinates.

$$\begin{aligned} t_s &= \ell / R_e \cdot \omega_0 \\ v_e &= \omega_e \cdot R_e \cos \phi \end{aligned}$$

and the entire effect is a function of, or linearly proportional to, the image x'' -dimension, as we see from Figure D.7.



Thus each y'' is shifted by $\Delta y''$:

$$\Delta y'' = \frac{x''}{\ell \cos A} \cdot t_s v_e \quad \text{(D.7)}$$

Thus we find:

$$\begin{matrix} x \\ y \end{matrix} = \begin{bmatrix} 1 & 0 \\ a & 1 \end{bmatrix} \begin{bmatrix} x'' \\ y'' \end{bmatrix} \quad \text{(D.8)}$$

Figure D.7: Effect of earth rotation on x'' , y'' is unaffected.

Where "a" results from (D.7) in conjunction with (D.4) and (D.5):

$$a = \frac{1}{l \cos A} \cdot \frac{l}{R_e \omega_o} \cdot R_e \cdot \cos \phi \cdot \omega_e \quad (D.9)$$

$$a = \frac{\cos \phi}{\cos A} \cdot \frac{\omega_e}{\omega_o} \quad (D.10)$$

Should the skew-correction be applied prior to the rotation for angle A, then

$$\Delta y' = t_s \cdot v_e \cdot x/l = x' \omega_e \cdot R_e \cos \phi \cdot l / (R_e \cdot \omega_o \cdot l)$$

$$\Delta y' = x' \omega_e \cdot \cos \phi / \omega_o \approx x' \cdot 0.07 \cdot \cos \phi \quad (D.11)$$

This needs to be applied to each 6-tuple of scan-lines jointly. Thus each six lines are treated as one, as shown in Figure D.8.

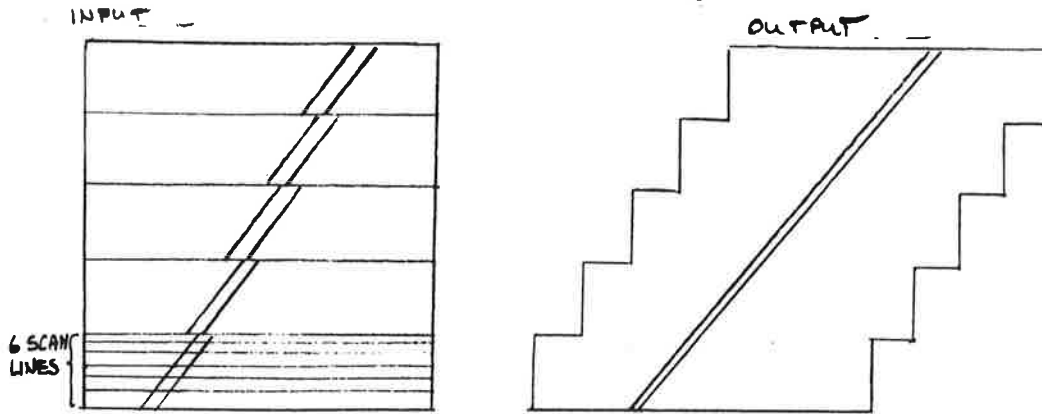


Figure D.8: Displacement of 6 scan lines due to Earth rotation.

D.7 Comments

It has been shown by many authors, that ground control points are required to correct severe image deformations. Therefore a separate panoramic, orbit inclination etc. correction does not seem to be overly meaningful. However, the 6-line skewing effect of Earth rotation must be corrected separately, because otherwise one leaves an unacceptable image degradation.

Depending on the receiving station's pre-processing one may or may not have to do the above corrections.